A Noise-to-State Stable Symmetry-Preserving Reduced-Order Observer for Wind Estimation

Jeremy W. Hopwood* and Craig A. Woolsey†
Virginia Tech, Blacksburg, VA 24061

Inferring wind velocity from aircraft motion is an enabling technology that can be used for synthetic air data systems, path planning, safety monitoring, and atmospheric science. This paper presents a reduced-order nonlinear wind observer applicable to uncertain aircraft models in turbulent wind. The aircraft dynamics are formulated as a stochastic differential equation that is invariant under the action of a Lie group. The proposed observer leverages this symmetry to achieve linear error dynamics that are shown to be noise-to-state stable in probability. A Monte-Carlo simulation of a nonlinear multirotor aircraft model is conducted to demonstrate the probabilistic guarantees and evaluate their conservatism.

I. Introduction

Inferring wind velocity from aircraft motion is an enabling technology across a wide range of applications. In aeronautics, wind estimates can be used in synthetic air data systems [1, 2] and path planning algorithms [3, 4]. Furthermore, with the accuracy of wind estimates quantified [5] and/or their convergence guaranteed [6], wind estimation algorithms can be incorporated into safety monitoring systems, such as [7] and [8], to replace traditional measurement techniques. Closely tied to aviation, wind estimates are also vital to weather prediction and atmospheric science [9–12]. These areas of application have become intertwined, especially within the poorly sampled atmospheric boundary layer, with advances in the Urban/Advanced Air Mobility (UAM/AAM) mission [13, 14]. For example, the development of wind estimation technologies is important in relaxing margins for flight safety to enable more weather-tolerant operations [15, 16].

The development of model-based wind estimation algorithms has brought finer temporal resolution and greater accuracy to wind velocity estimates [6, 17–19]. These *indirect* approaches feature a low instrumentation barrier as they do not require specialized sensors, such as an anemometer, to measure wind velocity. Instead, a model of the aircraft dynamics is used in conjunction with standard navigational sensors (e.g., accelerometer, gyroscope, magnetometer, and GNSS) to continuously estimate wind velocity at the aircraft's location.

The accuracy and stability of wind estimation methods are often limited by the assumptions underlying their approximations. We identify two key challenges to address. First, is the small-perturbation assumption that allows a linear flight dynamic model to be used with linear state estimators (e.g., the Kalman filter) and observers (e.g., the H_∞ filter). (The distinction between estimators and observers is made clear in the Appendix.) Even approximate nonlinear filter techniques such as the extended Kalman filter only retain their formal guarantees for small perturbations about steady motion with sufficiently low noise [20, 21]. For model-based wind estimation, nonlinear approaches that relax the small perturbation assumption are limited, but there have been some promising developments such as the nonlinear, passivity-based observer detailed in [6]. Another approach – the invariant extended Kalman filter – aims to expand the set of trajectories for which local stability is verified [22, 23]. These so-called *permanent trajectories* are a generalization of steady motions for which stability is guaranteed.

The second challenge in guaranteeing stability of wind estimation algorithms is how random disturbances are treated. Atmospheric turbulence is a random process (see [24, Ch. 13] and [25]) that casts the aircraft equations of motion in a stochastic setting. It is thus important to accurately model its effect on the aircraft dynamics when designing an observer or estimator. Kalman filter-based wind estimators inherently possess local stochastic stability guarantees [20]; however, the explicit stochastic stability guarantees of wind estimation algorithms are generally unexplored – especially for nonlinear observers.

To address these challenges and the shortcomings of previous approaches, we present a nonlinear state observer for aircraft flying in turbulent wind that enjoys stochastic stability guarantees. That is, we are able to make probabilistic statements about the convergence of state/wind estimates for the nonlinear dynamics – a powerful result that can

*Ph.D. Candidate, Kevin T. Crofton Department of Aerospace and Ocean Engineering, AIAA Student Member, jeremyhopwood@vt.edu
†Professor, Kevin T. Crofton Department of Aerospace and Ocean Engineering, AIAA Associate Fellow, cwoolsey@vt.edu

be used in all of the aforementioned applications. This observer is not of the typical Luenberger type, but rather is formulated using an immersion and invariance approach [26, 27]. The resulting reduced-order observer is symmetry-preserving [28, 29], and the state estimate error dynamics are linear so that optimal estimation methods may be readily employed. Finally, since the aircraft is subject to random turbulence and modeling error, results from the theory of noise-to-state stability [30] for stochastic differential equations are used to obtain probabilistic guarantees that the first two statistical moments of the state estimate error exponentially converge to a neighborhood of the origin.

This paper is organized as follows. Section II introduces the uncertain aircraft dynamics in turbulence and casts them as a stochastic differential equation (SDE). In Section III, a notion of SDE invariance under Lie group actions is introduced – a property the aircraft dynamics are shown to possess. The proposed symmetry-preserving reduced-order observer is presented in Section IV. Finally, the observer is demonstrated on simulated flight data for a multirotor aircraft in Section V, followed by concluding remarks in Section VI.

II. Stochastic Aircraft Dynamics in Turbulent Wind

A. Rigid-Body Kinematics on $\mathsf{TSE}(3)$

Consider an aircraft, modeled as a rigid body of mass m. Let the orthonormal vectors $\{\boldsymbol{i}_1, \boldsymbol{i}_2, \boldsymbol{i}_3\}$ define an earth-fixed North-East-Down (NED) reference frame, $\mathcal{F}_{\mathrm{I}}$, which we take to be inertial over the time and space scales of vehicle motion. Let the orthonormal vectors $\{\boldsymbol{b}_1, \boldsymbol{b}_2, \boldsymbol{b}_3\}$ define the body-fixed frame, $\mathcal{F}_{\mathrm{B}}$, centered at the aircraft center of gravity (CG) with $\boldsymbol{b}_1$ out the front of the aircraft, $\boldsymbol{b}_2$ out the right-hand side, and $\boldsymbol{b}_3$ out the bottom completing the right-handed frame. The position of the body frame with respect to the inertial frame is given by the vector $\boldsymbol{q} = [x\ y\ z]^{\mathsf{T}} \in \mathbb{R}^3$. The attitude of the aircraft is described by the rotation matrix $\boldsymbol{R}_{\mathrm{IB}} \in \mathsf{SO}(3)$ that maps free vectors from $\mathcal{F}_{\mathrm{B}}$ to $\mathcal{F}_{\mathrm{I}}$. The aircraft's configuration is described by points $(\boldsymbol{q}, \boldsymbol{R}_{\mathrm{IB}})$ in the special Euclidean group, $\mathsf{SE}(3) = \mathbb{R}^3 \rtimes \mathsf{SO}(3)$, where $\rtimes$ is the semi-direct product which expresses how two elements of the group compose a new element [31, §9.6]. Let $\boldsymbol{v} = [u\ v\ w]^{\mathsf{T}}$ and $\boldsymbol{\omega} = [p\ q\ r]^{\mathsf{T}}$ be the translational and rotational velocity of the aircraft with respect to $\mathcal{F}_{\mathrm{I}}$ expressed in $\mathcal{F}_{\mathrm{B}}$, respectively. The kinematic equations of motion are

$$\dot{\boldsymbol{q}} = \boldsymbol{R}_{\mathrm{IB}}\boldsymbol{v} \tag{1a}$$

$$\dot{\boldsymbol{R}}_{\mathrm{IB}} = \boldsymbol{R}_{\mathrm{IB}}\boldsymbol{S}(\boldsymbol{\omega}) \tag{1b}$$

where $\boldsymbol{S}(\cdot)$ is the skew-symmetric cross product equivalent matrix satisfying $\boldsymbol{S}(\boldsymbol{a})\boldsymbol{b} = \boldsymbol{a} \times \boldsymbol{b}$ for 3-vectors $\boldsymbol{a}$ and $\boldsymbol{b}$. Similarly, $\boldsymbol{S}^{-1}(\cdot)$ gives the vector whose cross product equivalent matrix is $(\cdot)$; that is, $\boldsymbol{S}^{-1}(\boldsymbol{S}(\boldsymbol{a})) = \boldsymbol{a}$. Geometrically, these kinematics are defined on the tangent bundle $\mathsf{TSE}(3) = \bigcup_{\boldsymbol{p}\in\mathsf{SE}(3)} \mathsf{T}_{\boldsymbol{p}}\mathsf{SE}(3)$, where $\mathsf{T}_{\boldsymbol{p}}\mathsf{SE}(3)$ denotes the tangent space to $\mathsf{SE}(3)$ at the point $\boldsymbol{p}$.

B. Stochastic Aircraft Dynamics in Turbulent Wind

Since the aim is to estimate wind velocity, we now consider aircraft motion in a time-varying wind field, $\boldsymbol{W} : \mathbb{R}^3 \times \mathbb{R} \to \mathbb{R}^3$, defined in the inertial frame. We will append the *apparent wind*

$$\boldsymbol{w}(t) = \boldsymbol{W}(\boldsymbol{q}(t), t) \tag{2}$$

to the aircraft state, where $\boldsymbol{w}$ is the part of the aircraft's extended state defined by evaluating the wind field $\boldsymbol{W}$ at the aircraft's position $\boldsymbol{q}$ at time t. Using the chain rule and assuming the vehicle does not affect the flow field in which it is immersed, the time derivative of $\boldsymbol{w}$ is

$$\frac{\mathrm{d}\boldsymbol{w}}{\mathrm{d}t} = \frac{\partial \boldsymbol{W}}{\partial t}(\boldsymbol{q}, t) + \nabla \boldsymbol{W}(\boldsymbol{q}, t)\frac{\mathrm{d}\boldsymbol{q}}{\mathrm{d}t} \tag{3}$$

While no general expression for the right-hand side of Eq. (3) is obtainable, noise shaping filters such as Dryden or Von Kármán turbulence models are often used to empirically model $\dot{\boldsymbol{w}}$ so that the spectral content of $\boldsymbol{w}$ resembles the wind experienced by an aircraft. For simplicity of presentation, however, we lump the right-hand side of Eq. (3) into a Brownian motion model for the purpose of observer design.

Assumption 1. *The apparent wind velocity is Brownian motion. Specifically, $\dot{\boldsymbol{w}} = \boldsymbol{\sigma}_w \dot{\boldsymbol{\mathcal{W}}}_w$, where $\dot{\boldsymbol{\mathcal{W}}}_w$ is unit variance, continuous-time, white noise and $\boldsymbol{\sigma}_w \boldsymbol{\sigma}_w^{\mathsf{T}}$ is the power spectral density of $\dot{\boldsymbol{w}}$.*

The aerodynamics of the aircraft depend on the body's air-relative velocity,

$$\boldsymbol{v}_{\mathrm{r}} = \boldsymbol{v} - \boldsymbol{R}_{\mathrm{IB}}^{\mathsf{T}} \boldsymbol{w} \tag{4}$$

rather than the inertial $\boldsymbol{v}$. Equation (4) is known as the *wind triangle*. Note that Eq. (3) represents the wind that would exist at the aircraft center of mass, if the aircraft were absent. Variations in wind velocity over the length and span of the aircraft are not captured by the pointwise expression (4), but they can be accounted for, to first order, by computing the wind gradient at $\boldsymbol{q}$ and t and assuming this gradient remains constant over the aircraft. For the purpose of wind observer design, however, we consider the following assumption about the rotational motion of the wind about the aircraft.

Assumption 2. *Wind gradients on the scale of the aircraft are considered to be an additive random disturbance. In particular, the air-relative angular velocity, $\boldsymbol{\omega}_{\mathrm{r}}$, can be taken to be equal to the body angular velocity, $\boldsymbol{\omega}$, in the aircraft dynamics by modeling the apparent body-frame wind angular velocity $\boldsymbol{\omega}_w = \boldsymbol{\omega} - \boldsymbol{\omega}_{\mathrm{r}}$ as a random process.*

Critically, the combination of Assumptions 1 and 2 allows us to neglect the effects of wind gradients in the observer design while not completely ignoring them in the observer stability/convergence guarantees.

Let us denote the aerodynamic force and moment acting on the aircraft expressed in $\mathcal{F}_{\mathrm{B}}$ as $\boldsymbol{F}$ and $\boldsymbol{M}$, respectively. Considering the force model for illustrative purposes, we in general have

$$\boldsymbol{F} = \mathfrak{F}(\boldsymbol{v}_{\mathrm{r}}, \boldsymbol{\omega}, \boldsymbol{\delta}; \boldsymbol{\vartheta}) + \text{parametric error} + \text{unmodeled dynamics} + \text{local gradient effects} \tag{5}$$

where $\mathfrak{F}$ is an aerodynamic model that smoothly depends on its arguments, $\boldsymbol{\delta}$ is the vector of known aircraft control inputs, and $\boldsymbol{\vartheta}$ is the vector of (imperfectly) identified model parameters. As seen in Eq. (5), the true force differs from the modeled force by parametric error, unmodeled dynamics, and local wind gradients (Assumption 2). For a well hypothesized and identified model, the parametric error is typically minimized and the unmodeled dynamics tend to resemble white, Gaussian noise [32]. Therefore, we can model the combination of these sources of uncertainty as a random process with known statistics. By the smoothness of $\mathfrak{F}$, we can write

$$\mathfrak{F}(\boldsymbol{v}_{\mathrm{r}}, \boldsymbol{\omega}, \boldsymbol{\delta}) = \boldsymbol{F}_0(\boldsymbol{v}_{\mathrm{r}}, \boldsymbol{\omega}, \boldsymbol{\delta}) + \boldsymbol{F}_v(\boldsymbol{v}_{\mathrm{r}}, \boldsymbol{\omega}, \boldsymbol{\delta})\boldsymbol{v}_{\mathrm{r}} + \boldsymbol{F}_\omega(\boldsymbol{v}_{\mathrm{r}}, \boldsymbol{\omega}, \boldsymbol{\delta})\boldsymbol{\omega} \tag{6}$$

These observations suggest the following assumption.

Assumption 3. *The aircraft's aerodynamic force and moment satisfy*

$$\boldsymbol{F} = \boldsymbol{F}_0 + \boldsymbol{F}_v \boldsymbol{v}_{\mathrm{r}} + \boldsymbol{F}_\omega \boldsymbol{\omega} + \Delta \boldsymbol{F} \tag{7}$$

$$\boldsymbol{M} = \boldsymbol{M}_0 + \boldsymbol{M}_v \boldsymbol{v}_{\mathrm{r}} + \boldsymbol{M}_\omega \boldsymbol{\omega} + \Delta \boldsymbol{M} \tag{8}$$

where $\boldsymbol{F}_{(\cdot)}$ and $\boldsymbol{M}_{(\cdot)}$ are known parameters that vary with the aircraft state and control, and $\Delta\boldsymbol{F}$ and $\Delta\boldsymbol{M}$ are zero-mean, Gaussian, white noise with known power spectral density.

The condition in Assumption 3 can be obtained by setting the arguments of $\boldsymbol{F}_{(\cdot)}$ and $\boldsymbol{M}_{(\cdot)}$ in Eq. (6) to their best-known values at the current time and lumping everything else into the assumed zero-mean, Gaussian, white modeling error terms $\Delta\boldsymbol{F}$ and $\Delta\boldsymbol{M}$.

Taking $\boldsymbol{I}$ to be the moment of inertia matrix of the rigid body about the center of mass in $\mathcal{F}_{\mathrm{B}}$ and letting $\boldsymbol{g}$ be the gravitational acceleration vector, one obtains the following extended state dynamic model for flight in random wind.

$$\dot{\boldsymbol{q}} = \boldsymbol{R}_{\mathrm{IB}} \boldsymbol{v}_{\mathrm{r}} + \boldsymbol{w} \tag{9a}$$

$$\dot{\boldsymbol{R}}_{\mathrm{IB}} = \boldsymbol{R}_{\mathrm{IB}} \boldsymbol{S}(\boldsymbol{\omega}) \tag{9b}$$

$$\dot{\boldsymbol{\omega}} = \boldsymbol{I}^{-1}\big(\boldsymbol{I}\boldsymbol{\omega} \times \boldsymbol{\omega} + \boldsymbol{M}_0 + \boldsymbol{M}_v \boldsymbol{v}_{\mathrm{r}} + \boldsymbol{M}_\omega \boldsymbol{\omega} + \Delta \boldsymbol{M}\big) \tag{9c}$$

$$\dot{\boldsymbol{v}}_{\mathrm{r}} = \boldsymbol{v}_{\mathrm{r}} \times \boldsymbol{\omega} + \boldsymbol{R}_{\mathrm{IB}}^{\mathsf{T}} \boldsymbol{g} + \frac{1}{m}\big(\boldsymbol{F}_0 + \boldsymbol{F}_v \boldsymbol{v}_{\mathrm{r}} + \boldsymbol{F}_\omega \boldsymbol{\omega} + \Delta \boldsymbol{F}\big) - \boldsymbol{R}_{\mathrm{IB}}^{\mathsf{T}} \dot{\boldsymbol{w}} \tag{9d}$$

$$\dot{\boldsymbol{w}} = \boldsymbol{\sigma}_w \dot{\boldsymbol{\mathcal{W}}}_w \tag{9e}$$

Assumption 4. *The aircraft's position ($\boldsymbol{q}$), attitude ($\boldsymbol{R}_{\mathrm{IB}}$), and angular velocity ($\boldsymbol{\omega}$) are measured without error.*

Thus, we take $\boldsymbol{y} = (\boldsymbol{q}, \boldsymbol{R}_{\mathrm{IB}}, \boldsymbol{\omega}) \in \mathcal{Y} = \mathsf{SE}(3) \times \mathbb{R}^3$ to be the measured part of the state and $\boldsymbol{x} = (\boldsymbol{v}_{\mathrm{r}}, \boldsymbol{w}) \in \mathcal{X} = \mathbb{R}^n$ to be the unmeasured part. Here, the dimension of $\mathcal{Y}$ is $m = 9$ ($\mathsf{SE}(3)$ is a 6-dimensional smooth manifold), and the dimension of $\mathcal{X}$ is $n = 6$. The total state space of the system is the $(n + m = 15)$-dimensional manifold $\mathcal{X} \times \mathcal{Y}$. We use the notation $(\boldsymbol{a}, \boldsymbol{b})$ as shorthand for $[\boldsymbol{a}^{\mathsf{T}}\ \boldsymbol{b}^{\mathsf{T}}]^{\mathsf{T}}$ when $\boldsymbol{a}$ and $\boldsymbol{b}$ are column vectors and more generally to denote points in the appropriate product space in which $\boldsymbol{a}$ and $\boldsymbol{b}$ belong.

The dynamics (9) are more formally viewed as a *stochastic differential equation* (SDE) defined on a complete probability space $(\Omega, \mathcal{F}, \mathbb{P})$. Here, we may identify Ω with the space of $\mathbb{R}^q$-valued continuous functions $\boldsymbol{\mathcal{W}}(t)$ on $[0, \infty)$. For fixed $\omega \in \Omega$, $\boldsymbol{\mathcal{W}}(t, \omega)$ is called a *sample path* of the random process $\boldsymbol{\mathcal{W}}(t)$. The sigma algebra $\mathcal{F}$ collects all measurable subsets of Ω to form the measurable space $(\Omega, \mathcal{F})$ on which we assign a probability measure $\mathbb{P} : \mathcal{F} \to [0, 1]$ such that $\boldsymbol{\mathcal{W}}$ is a standard Wiener process [33]*. The increments of the driving Wiener process $\boldsymbol{\mathcal{W}} = (\boldsymbol{\mathcal{W}}_w, \boldsymbol{\mathcal{W}}_M, \boldsymbol{\mathcal{W}}_F)$ of the stochastic aircraft dynamics (9) satisfy

$$\mathrm{d}\boldsymbol{w} = \boldsymbol{\sigma}_w \mathrm{d}\boldsymbol{\mathcal{W}}_w, \qquad \boldsymbol{I}^{-1}\Delta\boldsymbol{M}\mathrm{d}t = \boldsymbol{\sigma}_M \mathrm{d}\boldsymbol{\mathcal{W}}_M, \qquad \frac{1}{m}\Delta\boldsymbol{F}\mathrm{d}t = \boldsymbol{\sigma}_F \mathrm{d}\boldsymbol{\mathcal{W}}_F \tag{10}$$

Using Eq. (10), we may more formally write Eqs. (9c)–(9e) as the SDE

$$\mathrm{d}\boldsymbol{\omega} = \boldsymbol{I}^{-1}\big(\boldsymbol{I}\boldsymbol{\omega} \times \boldsymbol{\omega} + \boldsymbol{M}_0 + \boldsymbol{M}_v\boldsymbol{v}_{\mathrm{r}} + \boldsymbol{M}_\omega\boldsymbol{\omega}\big)\mathrm{d}t + \boldsymbol{\sigma}_M \mathrm{d}\boldsymbol{\mathcal{W}}_M \tag{11a}$$

$$\mathrm{d}\boldsymbol{v}_{\mathrm{r}} = \Big(\boldsymbol{v}_{\mathrm{r}} \times \boldsymbol{\omega} + \boldsymbol{R}_{\mathrm{IB}}^{\mathsf{T}}\boldsymbol{g} + \frac{1}{m}\big(\boldsymbol{F}_0 + \boldsymbol{F}_v\boldsymbol{v}_{\mathrm{r}} + \boldsymbol{F}_\omega\boldsymbol{\omega}\big)\Big)\mathrm{d}t + \boldsymbol{\sigma}_F \mathrm{d}\boldsymbol{\mathcal{W}}_F - \boldsymbol{R}_{\mathrm{IB}}^{\mathsf{T}}\boldsymbol{\sigma}_w \mathrm{d}\boldsymbol{\mathcal{W}}_w \tag{11b}$$

$$\mathrm{d}\boldsymbol{w} = \boldsymbol{\sigma}_w \mathrm{d}\boldsymbol{\mathcal{W}}_w \tag{11c}$$

The kinematics on $\mathsf{SE}(3)$ are not included in the SDE (11) since they are not Euclidean. However, such a technical distinction† does not matter since we are not concerned about statistics of $(\boldsymbol{q}, \boldsymbol{R}_{\mathrm{IB}})$ and can always choose local coordinates for $\mathsf{SE}(3)$ so that (through a minor abuse of notation) the stochastic aircraft dynamics (9) are written as

$$\mathrm{d}\boldsymbol{x} = \boldsymbol{f}(\boldsymbol{x}, \boldsymbol{y}, \boldsymbol{u})\mathrm{d}t + \boldsymbol{G}_x(\boldsymbol{y})\boldsymbol{\sigma}\mathrm{d}\boldsymbol{\mathcal{W}} \tag{12a}$$

$$\mathrm{d}\boldsymbol{y} = \boldsymbol{h}(\boldsymbol{x}, \boldsymbol{y}, \boldsymbol{u})\mathrm{d}t + \boldsymbol{G}_y\boldsymbol{\sigma}\mathrm{d}\boldsymbol{\mathcal{W}} \tag{12b}$$

where $(\boldsymbol{f}, \boldsymbol{h})$ is the *drift vector field* and $(\boldsymbol{G}_x, \boldsymbol{G}_y)$ is the *diffusion matrix field*, both constructed from the right-hand side of Eq. (9) using Eq. (10). The matrix $\boldsymbol{\sigma} = \mathbf{diag}(\boldsymbol{\sigma}_w, \boldsymbol{\sigma}_M, \boldsymbol{\sigma}_F) \in \mathbb{R}^{9\times 9}$ is defined such that $\boldsymbol{\sigma}\boldsymbol{\sigma}^{\mathsf{T}}$ is the *infinitesimal covariance* of the Brownian motion $\boldsymbol{\sigma}\boldsymbol{\mathcal{W}}$. In Eq. (12), $\boldsymbol{u}$ is the known "input" to the system. It is not necessarily just control inputs, but rather a collection of known quantities on which a particular transformation group acts (as will be detailed in Section III). In our case, it is simply $\boldsymbol{u} = \boldsymbol{g}$. The formulation of the aircraft dynamics (9) as the SDE (12) will allow us to eventually make probabilistic statements on the convergence of the estimate of $\boldsymbol{x}$ to its true value.

III. Invariance of the Stochastic Aircraft Dynamics

In order to design a symmetry-preserving observer for the aircraft in wind, we must determine what transformations of the aircraft state, input, and noise leave the dynamics (9) unchanged – that is, *invariant*. Previously, this concept has only been applied to observer design for *ordinary* differential equations.

A. Mathematical Preliminaries

Consider the following preliminaries on invariant theory for ODEs (Section III.A.1) and Itô calculus (Section III.A.2).

1. G-Invariance of Ordinary Differential Equations [36, 37]

A Lie group G is said to *act* on a manifold $\mathcal{X}$ via the mapping

$$\boldsymbol{\varphi} : G \times \mathcal{X} \to \mathcal{X},\ (g, \boldsymbol{x}) \mapsto \boldsymbol{\varphi}_g(\boldsymbol{x}) \tag{13}$$

if (i) the identity element e in G induces the identity transformation $\boldsymbol{\varphi}_e(\boldsymbol{x}) = \boldsymbol{x}$ for all $\boldsymbol{x} \in \mathcal{X}$, and (ii) the composition of group actions satisfies $\boldsymbol{\varphi}_g \circ \boldsymbol{\varphi}_h = \boldsymbol{\varphi}_{g*h}$, where "$\circ$" denotes the composition of mappings and "$*$" is group

*The interested reader is directed to [34] for a concise introduction to SDEs.

†Stochastic dynamics on non-Euclidean manifolds are defined by sections of *Itô bundles* [35] – not the more conventional tangent bundle.

multiplication [36, 37]. Note the inverse transformation $\boldsymbol{\varphi}_g^{-1}$ is given by the action of the inverse group element – i.e., $\boldsymbol{\varphi}_g^{-1} = \boldsymbol{\varphi}_{g^{-1}}$. With these properties, the collection $\{\boldsymbol{\varphi}_g\}_{g\in G}$ is called a *transformation group*.

As explained in [29, 37], a dynamical control system

$$\dot{\boldsymbol{x}} = \boldsymbol{f}(\boldsymbol{x}, \boldsymbol{u}) \tag{14}$$

is called G-*invariant* with respect to the transformation group $\{\boldsymbol{\varphi}_g, \boldsymbol{\psi}_g\}_{g\in G}$ if

$$\boldsymbol{f}(\boldsymbol{\varphi}_g(\boldsymbol{x}), \boldsymbol{\psi}_g(\boldsymbol{u})) = \mathrm{T}\boldsymbol{\varphi}_g(\boldsymbol{x}) \cdot \boldsymbol{f}(\boldsymbol{x}, \boldsymbol{u}) \tag{15}$$

where $\mathrm{T}\boldsymbol{\varphi}_g(\boldsymbol{x}) : \mathsf{T}_{\boldsymbol{x}}\mathcal{X} \to \mathsf{T}_{\boldsymbol{\varphi}_g(\boldsymbol{x})}\mathcal{X}$ denotes the *tangent map* of $\boldsymbol{\varphi}_g$ at $\boldsymbol{x}$ and "$\cdot$" denotes its application to a tangent vector. Note if $\mathcal{X} = \mathbb{R}^n$, then $\mathrm{T}\boldsymbol{\varphi}_g(\boldsymbol{x})$ is simply the Jacobian matrix, $\partial\boldsymbol{\varphi}_g(\boldsymbol{x})/\partial\boldsymbol{x}$.

2. Stochastic Differential Equations and Itô's Rule [33, 34]

On a complete probability space $(\Omega, \mathcal{F}, \mathbb{P})$, consider the SDE

$$\mathrm{d}\boldsymbol{x} = \boldsymbol{f}(t, \boldsymbol{x})\mathrm{d}t + \boldsymbol{G}(t, \boldsymbol{x})\boldsymbol{\sigma}\mathrm{d}\boldsymbol{\mathcal{W}} \tag{16}$$

written in the sense of Itô. That is, Eq. (16) is shorthand for

$$\boldsymbol{x}(t) = \boldsymbol{x}(0) + \int_0^t \boldsymbol{f}(s, \boldsymbol{x}(s))\mathrm{d}s + \int_0^t \boldsymbol{G}(s, \boldsymbol{x}(s))\boldsymbol{\sigma}\mathrm{d}\boldsymbol{\mathcal{W}}(s) \tag{17}$$

where $\int_0^t \boldsymbol{f}(s, \boldsymbol{x}(s))\mathrm{d}s$ is the standard Lebesgue integral and $\int_0^t \boldsymbol{G}(s, \boldsymbol{x}(s))\boldsymbol{\sigma}\mathrm{d}\boldsymbol{\mathcal{W}}(s)$ is the Itô integral with respect to the standard Wiener process $\boldsymbol{\mathcal{W}}$. Functions of the random process (17) do not follow the typical chain rule, but instead obey Itô's rule/lemma.

Lemma 1 (Itô's Lemma)**.** *Given a random process $\boldsymbol{x}$ satisfying Eq.* (17) *and a function $V(t, \boldsymbol{x})$ that is once differentiable in t and twice differentiable in $\boldsymbol{x}$, the random process $v = V(t, \boldsymbol{x})$ satisfies*

$$\mathrm{d}v = \left(\frac{\partial V}{\partial t} + \frac{\partial V}{\partial \boldsymbol{x}}\boldsymbol{f} + \frac{1}{2}\,\mathrm{Tr}\left[\boldsymbol{\sigma}^{\mathsf{T}}\boldsymbol{G}^{\mathsf{T}}\frac{\partial^2 V}{\partial \boldsymbol{x}^2}\boldsymbol{G}\boldsymbol{\sigma}\right]\right)\mathrm{d}t + \frac{\partial V}{\partial \boldsymbol{x}}\boldsymbol{G}\boldsymbol{\sigma}\mathrm{d}\boldsymbol{\mathcal{W}} \tag{18}$$

Even though we cannot just "divide by $\mathrm{d}t$" in Eq. (18) to get $\dot{v}$ ($\boldsymbol{\mathcal{W}}$ is differentiable nowhere), we still need a notion of the rate-of-change of v. This motivates the definition of a linear operator called the *infinitesimal generator* $\mathscr{L}$ of the random process $\boldsymbol{x}(t)$. For SDEs [38], the infinitesimal generator satisfies

$$\mathscr{L}V = \frac{\partial V}{\partial \boldsymbol{x}}\boldsymbol{f} + \frac{1}{2}\,\mathrm{Tr}\left[\boldsymbol{\sigma}^{\mathsf{T}}\boldsymbol{G}^{\mathsf{T}}\frac{\partial^2 V}{\partial \boldsymbol{x}^2}\boldsymbol{G}\boldsymbol{\sigma}\right] \tag{19}$$

If $\mathscr{L}$ is applied to a vector-valued function, it is computed element-wise. Using $\mathscr{L}$, Itô's rule (18) may be equivalently written as

$$\mathrm{d}v = \left(\frac{\partial V}{\partial t} + \mathscr{L}V\right)\mathrm{d}t + \frac{\partial V}{\partial \boldsymbol{x}}\boldsymbol{G}\boldsymbol{\sigma}\mathrm{d}\boldsymbol{\mathcal{W}} \tag{20}$$

Since increments $\mathrm{d}\boldsymbol{\mathcal{W}}$ of the Wiener process are zero-mean, the expected rate of change of v is $\partial V/\partial t + \mathscr{L}V$ – a fact we will use in the Lyapunov stability analysis presented in Section IV.C.

B. G-Invariance of Stochastic Differential Equations

Similar to [39], we propose the following definition of G-invariance for controlled SDEs.

Definition 1 (G-invariant SDE)**.** *Suppose the Lie group G acts on the SDE*

$$\mathrm{d}\boldsymbol{x} = \boldsymbol{f}(\boldsymbol{x}, \boldsymbol{u})\mathrm{d}t + \boldsymbol{G}(\boldsymbol{x}, \boldsymbol{u})\boldsymbol{\sigma}\mathrm{d}\boldsymbol{\mathcal{W}} \tag{21}$$

via the transformation group

$$(g, \boldsymbol{x}, \boldsymbol{u}, \boldsymbol{\mathcal{W}}) \in G \times \mathcal{X} \times \mathcal{U} \times \mathbb{R}^q \mapsto (\boldsymbol{\varphi}_g(\boldsymbol{x}), \boldsymbol{\psi}_g(\boldsymbol{u}), \boldsymbol{\varpi}_g(\boldsymbol{\mathcal{W}})) \in \mathcal{X} \times \mathcal{U} \times \mathbb{R}^q$$

The SDE (21) *is called* G-invariant *if*

$$\mathrm{d}\boldsymbol{\varphi}_g(\boldsymbol{x}) = \boldsymbol{f}(\boldsymbol{\varphi}_g(\boldsymbol{x}), \boldsymbol{\psi}_g(\boldsymbol{u}))\mathrm{d}t + \boldsymbol{G}(\boldsymbol{\varphi}_g(\boldsymbol{x}), \boldsymbol{\psi}_g(\boldsymbol{u}))\mathrm{d}\boldsymbol{\varpi}_g(\boldsymbol{\mathcal{W}}) \tag{22}$$

where $\mathrm{d}\boldsymbol{\varphi}_g$ and $\mathrm{d}\boldsymbol{\varpi}_g$ are understood in the sense of Itô.

Comparing with Definition 1, the condition for G-invariance of deterministic systems may be written as $\mathrm{d}\boldsymbol{\varphi}_g(\boldsymbol{x})/\mathrm{d}t = \boldsymbol{f}(\boldsymbol{\varphi}_g(\boldsymbol{x}), \boldsymbol{\psi}_g(\boldsymbol{u}))$ [29], which differs from Definition 1 in the same way that $\dot{\boldsymbol{x}} = \boldsymbol{f}(\boldsymbol{x}, \boldsymbol{u})$ differs from $\mathrm{d}\boldsymbol{x} = \boldsymbol{f}(\boldsymbol{x}, \boldsymbol{u})\mathrm{d}t + \boldsymbol{G}(\boldsymbol{x}, \boldsymbol{u})\boldsymbol{\sigma}\mathrm{d}\boldsymbol{\mathcal{W}}$.

Here, we aim to find a transformation group $\{\boldsymbol{\varphi}_g, \boldsymbol{\varrho}_g, \boldsymbol{\psi}_g, \boldsymbol{\varpi}_g\}_{g\in G}$ for the SDE (12), where $\boldsymbol{\varphi}_g$ acts on the unmeasured part of state, $\boldsymbol{\varrho}_g$ acts on the measured part, $\boldsymbol{\psi}_g$ acts on the input, and $\boldsymbol{\varpi}_g$ acts on the Wiener process. Recall Lie groups are mathematical groups that are also smooth manifolds; that is, they are sets of elements that act on each other through group multiplication, but also topological spaces that correspond (locally) to Euclidean space. As described in Section II.A, the configuration of the rigid-body aircraft is a point on such a manifold – the special Euclidean group $\mathsf{SE}(3)$. Therefore, $\mathsf{SE}(3)$ is a natural choice of Lie group G for which a transformation group is defined (like in [22, 23]). However, since position does not explicitly appear on the right-hand side of Eq. 9, considering $G = \mathsf{SO}(3)$ is sufficient for the observer presented in this paper.

As explored in [40] for the deterministic case, there are two transformation groups we may consider. One acts on all quantities expressed in the body frame, while the other acts on inertial frame quantities. It was found in simulations that this *inertial transformation group* yielded slightly better results for the deterministic case. Therefore, we consider the following as its extension to the stochastic aircraft dynamics.

Proposition 1. *The stochastic aircraft dynamics represented by the SDE* (12) *are* $\mathsf{SO}(3)$*-invariant under the transformation group*

$$\begin{gathered}\boldsymbol{\varphi}_g(\boldsymbol{x}) = \begin{pmatrix}\boldsymbol{v}_{\mathrm{r}}\\ \boldsymbol{R}_g\boldsymbol{w}\end{pmatrix} =: \begin{pmatrix}\boldsymbol{\varphi}_g^{v_{\mathrm{r}}}(\boldsymbol{x})\\ \boldsymbol{\varphi}_g^{w}(\boldsymbol{x})\end{pmatrix}, \quad \boldsymbol{\varrho}_g(\boldsymbol{y}) = \begin{pmatrix}\boldsymbol{R}_g\boldsymbol{q}\\ \boldsymbol{R}_g\boldsymbol{R}_{\mathrm{IB}}\\ \boldsymbol{\omega}\end{pmatrix} =: \begin{pmatrix}\boldsymbol{\varrho}_g^{q}(\boldsymbol{y})\\ \boldsymbol{\varrho}_g^{R_{\mathrm{IB}}}(\boldsymbol{y})\\ \boldsymbol{\varrho}_g^{\omega}(\boldsymbol{y})\end{pmatrix}\\ \boldsymbol{\psi}_g(\boldsymbol{u}) = \boldsymbol{R}_g\boldsymbol{g}, \qquad \mathrm{d}\boldsymbol{\varpi}_g(\boldsymbol{\sigma}\boldsymbol{\mathcal{W}}) = \begin{pmatrix}\boldsymbol{R}_g\boldsymbol{\sigma}_w\mathrm{d}\boldsymbol{\mathcal{W}}_w\\ \boldsymbol{\sigma}_M\mathrm{d}\boldsymbol{\mathcal{W}}_M\\ \boldsymbol{\sigma}_F\mathrm{d}\boldsymbol{\mathcal{W}}_F\end{pmatrix} =: \begin{pmatrix}\mathrm{d}\boldsymbol{\varpi}_g^{w}(\boldsymbol{\sigma}\boldsymbol{\mathcal{W}})\\ \mathrm{d}\boldsymbol{\varpi}_g^{M}(\boldsymbol{\sigma}\boldsymbol{\mathcal{W}})\\ \mathrm{d}\boldsymbol{\varpi}_g^{F}(\boldsymbol{\sigma}\boldsymbol{\mathcal{W}})\end{pmatrix}\end{gathered} \tag{23}$$

where $g = \boldsymbol{R}_g \in \mathsf{SO}(3)$.

The proof of Proposition 1 is omitted for brevity. Its deterministic counterpart may be found in [40]. This transformation group characterizes the rotational symmetry of the aircraft dynamics. It recognizes the fact that the orientation of the inertial frame is arbitrary.

IV. Stochastic Symmetry-Preserving Reduced-Order Wind Observer

Now that we have established how the SDE (12) is $\mathsf{SO}(3)$-invariant, the theory developed in [28] for deterministic systems can be extended to obtain a reduced-order observer that preserves symmetries associated with transformation group (23).

A. The Moving Frame

To preserve symmetries in the observer dynamics, we make use of a *moving frame* [36, Ch. 8], which can be used to find invariant functions of the system's state. The moving frame is intimately tied to how sets of transformed points $\{\boldsymbol{\varrho}_g(\boldsymbol{y}) \in \mathcal{Y} \mid g \in G\}$, called *$G$-orbits*, relate to the composition of Lie group actions. For our problem, we only need to consider the transformation on the measured part of the state, $\boldsymbol{\varrho}_g(\boldsymbol{y})$. Therefore, it is sufficient to consider a *moving frame* to be a mapping $\gamma : \mathcal{Y} \to G$ that has the *equivariance* property

$$\gamma(\boldsymbol{\varrho}_g(\boldsymbol{y})) * g = \gamma(\boldsymbol{y}) \tag{24}$$

Geometrically, the moving frame may be viewed as the map from the state space to the Lie group element that transforms points to a chosen *cross-section* – a submanifold $\mathcal{K} \subseteq \mathcal{Y}$ that transversely intersects G-orbits on $\mathcal{Y}$. This interpretation provides a method for constructing a moving frame [29, 36], which we summarize as follows. For an r-dimensional Lie group G acting freely[‡] on the m-dimensional manifold $\mathcal{Y}$, let $\boldsymbol{\varrho}_g^{\mathrm{inv}}$ be the part of $\boldsymbol{\varrho}_g$ that maps points $\boldsymbol{y} \in \mathcal{Y}$ to an r-dimensional submanifold of $\mathcal{Y}$ such that $\boldsymbol{\varrho}_g^{\mathrm{inv}}$ is invertible with respect to g in a neighborhood of the identity element $e \in G$. Then, one can select a constant $\boldsymbol{k}$ in the image of $\boldsymbol{\varrho}_g^{\mathrm{inv}}$ that defines the unique point at which the

[‡]The Lie group G is said to *act freely* on $\mathcal{Y}$ if $\boldsymbol{\varrho}_g(\boldsymbol{y}) = \boldsymbol{y}$ implies g is the identity element, e.

G-orbit of a generic point $\boldsymbol{y}$ intersects the $(m-r)$-dimensional cross-section $\mathcal{K}$. In other words, the moving frame is obtained by solving the *normalization equation*

$$\boldsymbol{\varrho}_h^{\text{inv}}(\boldsymbol{y}) = \boldsymbol{k} \tag{25}$$

for $h \in G$. The local solution $h = \gamma(\boldsymbol{y})$ defines the moving frame, as depicted in Figure 1.

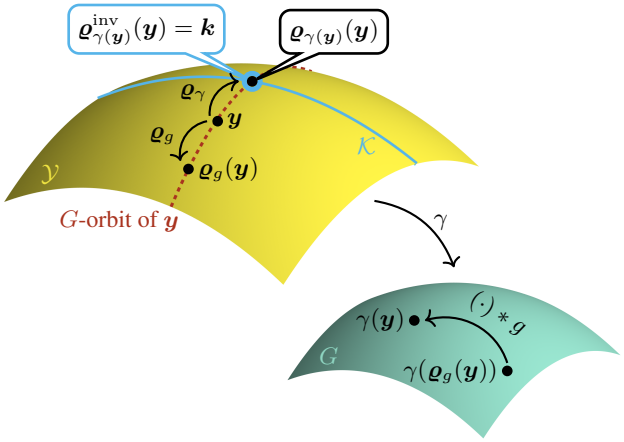

Fig. 1 Equivariance of the moving frame γ and its construction via the cross-section $\mathcal{K}$.

Since the attitude state space of the system is G itself, the *moving frame* $\gamma : \mathcal{Y} \to G$ is naturally defined by the element of $G = \mathsf{SO}(3)$ whose action on the rotational configuration yields the identity element, $e = \mathbb{I}$. Therefore, the normalization equation reads

$$\boldsymbol{R}_h \boldsymbol{R}_{\text{IB}} = \mathbb{I} \tag{26}$$

which implies

$$h = \gamma(\boldsymbol{y}) = \boldsymbol{R}_{\text{IB}}^{\mathsf{T}} \tag{27}$$

is the group element that defines a moving frame with the equivariance property (24). The moving frame will be used to construct an invariant mapping from the measured states to estimates of the unmeasured states, which is then used to define the form of the symmetry-preserving reduced-order observer (Section IV.B) and obtain sufficient conditions for its stability (Section IV.C).

B. Stochastic G-Invariant Pre-Observer

With moving frames identified, we can construct a symmetry-preserving reduced-order pre-observer, defined as follows.

Definition 2 (Pre-Observer)**.** *The dynamical system*

$$\dot{\boldsymbol{z}} = \boldsymbol{\alpha}(\boldsymbol{z}, \boldsymbol{y}, \boldsymbol{u}) \tag{28}$$

with output

$$\hat{\boldsymbol{x}} = \boldsymbol{z} + \boldsymbol{\beta}(\boldsymbol{y}) \tag{29}$$

for some smooth map $\boldsymbol{\beta} : \mathcal{Y} \to \mathcal{X}$ is a stochastic G-invariant reduced-order pre-observer for the system (12) *if the SDE*

$$\mathrm{d}\hat{\boldsymbol{x}} = \boldsymbol{\alpha}(\hat{\boldsymbol{x}} - \boldsymbol{\beta}(\boldsymbol{y}), \boldsymbol{y}, \boldsymbol{u})\mathrm{d}t + \mathrm{d}\boldsymbol{\beta}(\boldsymbol{y}) \tag{30}$$

is G-invariant and the manifold

$$\mathcal{Z} = \{(\boldsymbol{z}, \boldsymbol{x}, \boldsymbol{y}) \in \mathcal{X} \times \mathcal{X} \times \mathcal{Y} \mid \boldsymbol{z} = \boldsymbol{x} - \boldsymbol{\beta}(\boldsymbol{y})\} \tag{31}$$

is positively invariant under the flow of the drift vector field $(\boldsymbol{f}, \boldsymbol{h})$.

The key to constructing the pre-observer (28) is the choice of $\boldsymbol{\beta}$, which we call the *observer map*. Inspired by Lemma 1 in [28], let

$$\boldsymbol{\beta}(\boldsymbol{y}) = \boldsymbol{\varphi}_{\gamma(\boldsymbol{y})^{-1}}\Big(\boldsymbol{\ell}\big(\boldsymbol{\varrho}_{\gamma(\boldsymbol{y})}(\boldsymbol{y})\big)\Big) \tag{32}$$

where $\boldsymbol{\ell} : \mathcal{Y} \to \mathcal{X}$ is a smooth map. As illustrated in Figure 2, this choice of $\boldsymbol{\beta}$ is special in that it commutes with the transformation group. That is,

$$\boldsymbol{\varphi}_g(\boldsymbol{\beta}(\boldsymbol{y})) = \boldsymbol{\beta}(\boldsymbol{\varrho}_g(\boldsymbol{y})) \tag{33}$$

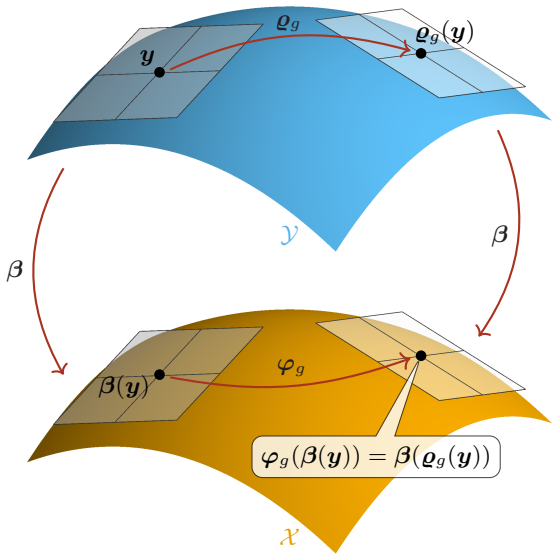

Fig. 2 Commutative relationship between $\boldsymbol{\beta}$ and the transformation group.

Inspecting the choice of $\boldsymbol{\beta}$ in Eq. (32), we notice that $\boldsymbol{\varrho}_{\gamma(\boldsymbol{y})}^{R_{\mathrm{IB}}}(\boldsymbol{y}) = \mathbb{I}$. Therefore, we need only consider $\boldsymbol{\ell} : \mathcal{Y} \setminus \mathsf{SO}(3) \to \mathcal{X}$. Let

$$\boldsymbol{\ell}(\boldsymbol{y}) = \underbrace{\begin{bmatrix} \boldsymbol{L}_{v_{\mathrm{r}}}^{q} & \boldsymbol{L}_{v_{\mathrm{r}}}^{\omega} \\ \boldsymbol{L}_{w}^{q} & \boldsymbol{L}_{w}^{\omega} \end{bmatrix}}_{\boldsymbol{L}} \begin{bmatrix} \boldsymbol{q} \\ \boldsymbol{\omega} \end{bmatrix} \tag{34}$$

where $\boldsymbol{L}$ is the *observer gain matrix* which we allow to vary with time. With this choice of $\boldsymbol{\ell}$, Eq. (32) becomes

$$\boldsymbol{\beta}(\boldsymbol{y}) = \begin{bmatrix} \boldsymbol{L}_{v_{\mathrm{r}}}^{q} \boldsymbol{R}_{\mathrm{IB}}^{\mathsf{T}} \boldsymbol{q} + \boldsymbol{L}_{v_{\mathrm{r}}}^{\omega} \boldsymbol{\omega} \\ \boldsymbol{R}_{\mathrm{IB}} \boldsymbol{L}_{w}^{q} \boldsymbol{R}_{\mathrm{IB}}^{\mathsf{T}} \boldsymbol{q} + \boldsymbol{R}_{\mathrm{IB}} \boldsymbol{L}_{w}^{\omega} \boldsymbol{\omega} \end{bmatrix} \tag{35}$$

As an extension of Theorem 1 in [28], consider the following proposition given without proof.

Proposition 2 (Pre-Observer)**.** *Let the vector field $\boldsymbol{\alpha}(\cdot, \boldsymbol{y}, \boldsymbol{u}) : \mathbb{R}^n \to \mathsf{T}\mathbb{R}^n$ be defined by*

$$\boldsymbol{\alpha}(\boldsymbol{z}, \boldsymbol{y}, \boldsymbol{u}) = \boldsymbol{f}(\boldsymbol{z} + \boldsymbol{\beta}(\boldsymbol{y}), \boldsymbol{y}, \boldsymbol{u}) - \mathscr{L}\boldsymbol{\beta}(\boldsymbol{y})|_{\boldsymbol{x}=\boldsymbol{z}+\boldsymbol{\beta}(\boldsymbol{y})} \tag{36}$$

Then, the dynamical system (28) *with output* (29) *is a stochastic G-invariant, reduced-order pre-observer.*

The components of $\boldsymbol{\alpha}$ as defined by Eq. (36) are

$$\begin{aligned} \boldsymbol{\alpha}_{v_{\mathrm{r}}}(\boldsymbol{z}, \boldsymbol{y}, \boldsymbol{u}) = \hat{\boldsymbol{v}}_{\mathrm{r}} \times \boldsymbol{\omega} + \boldsymbol{R}_{\mathrm{IB}}^{\mathsf{T}} \boldsymbol{g} + \frac{1}{m}\left(\boldsymbol{F}_0 + \boldsymbol{F}_v \hat{\boldsymbol{v}}_{\mathrm{r}} + \boldsymbol{F}_\omega \boldsymbol{\omega}\right) - \boldsymbol{L}_{v_{\mathrm{r}}}^{q} \boldsymbol{R}_{\mathrm{IB}}^{\mathsf{T}}\left(\boldsymbol{R}_{\mathrm{IB}} \hat{\boldsymbol{v}}_{\mathrm{r}} + \hat{\boldsymbol{w}}\right) \\ - \boldsymbol{L}_{v_{\mathrm{r}}}^{\omega} \boldsymbol{I}^{-1}\left(\boldsymbol{I}\boldsymbol{\omega} \times \boldsymbol{\omega} + \boldsymbol{M}_0 + \boldsymbol{M}_v \hat{\boldsymbol{v}}_{\mathrm{r}} + \boldsymbol{M}_\omega \boldsymbol{\omega}\right) + \boldsymbol{L}_{v_{\mathrm{r}}}^{q} \boldsymbol{S}(\boldsymbol{\omega}) \boldsymbol{R}_{\mathrm{IB}}^{\mathsf{T}} \boldsymbol{q} - \dot{\boldsymbol{L}}_{v_{\mathrm{r}}}^{q} \boldsymbol{R}_{\mathrm{IB}}^{\mathsf{T}} \boldsymbol{q} - \dot{\boldsymbol{L}}_{v_{\mathrm{r}}}^{\omega} \boldsymbol{\omega} \end{aligned} \tag{37a}$$

$$\boldsymbol{\alpha}_w(\boldsymbol{z},\boldsymbol{y},\boldsymbol{u}) = -\boldsymbol{R}_{\mathrm{IB}}\boldsymbol{L}_w^q\boldsymbol{R}_{\mathrm{IB}}^{\mathsf{T}}\left(\boldsymbol{R}_{\mathrm{IB}}\hat{\boldsymbol{v}}_{\mathrm{r}}+\hat{\boldsymbol{w}}\right)-\boldsymbol{R}_{\mathrm{IB}}\boldsymbol{L}_w^{\omega}\boldsymbol{I}^{-1}\left(\boldsymbol{I}\boldsymbol{\omega}\times\boldsymbol{\omega}+\boldsymbol{M}_0+\boldsymbol{M}_v\hat{\boldsymbol{v}}_{\mathrm{r}}+\boldsymbol{M}_{\omega}\boldsymbol{\omega}\right)$$
$$-\boldsymbol{R}_{\mathrm{IB}}\boldsymbol{S}(\boldsymbol{\omega})\boldsymbol{L}_w^{\omega}\boldsymbol{\omega}-\boldsymbol{R}_{\mathrm{IB}}\left(\boldsymbol{S}(\boldsymbol{\omega})\boldsymbol{L}_w^q-\boldsymbol{L}_w^q\boldsymbol{S}(\boldsymbol{\omega})\right)\boldsymbol{R}_{\mathrm{IB}}^{\mathsf{T}}\boldsymbol{q}-\boldsymbol{R}_{\mathrm{IB}}\dot{\boldsymbol{L}}_w^q\boldsymbol{R}_{\mathrm{IB}}^{\mathsf{T}}\boldsymbol{q}-\boldsymbol{R}_{\mathrm{IB}}\dot{\boldsymbol{L}}_w^{\omega}\boldsymbol{\omega} \quad (37b)$$

where

$$\begin{aligned}\hat{\boldsymbol{v}}_{\mathrm{r}} &= \boldsymbol{z}_{v_{\mathrm{r}}}+\boldsymbol{L}_{v_{\mathrm{r}}}^q\boldsymbol{R}_{\mathrm{IB}}^{\mathsf{T}}\boldsymbol{q}+\boldsymbol{L}_{v_{\mathrm{r}}}^{\omega}\boldsymbol{\omega}\\ \hat{\boldsymbol{w}} &= \boldsymbol{z}_w+\boldsymbol{R}_{\mathrm{IB}}\boldsymbol{L}_w^q\boldsymbol{R}_{\mathrm{IB}}^{\mathsf{T}}\boldsymbol{q}+\boldsymbol{R}_{\mathrm{IB}}\boldsymbol{L}_w^{\omega}\boldsymbol{\omega}\end{aligned} \quad (38)$$

Remark 1. *The expression for $\boldsymbol{\alpha}$ in Eq.* (37) *is the same as the deterministic observer in [40]. This is because $\boldsymbol{\beta}$ is linear in the states for which noise enters the stochastic dynamics* (9)*. Therefore, the Hessian in Itô's rule vanishes.*

The remaining task is to choose the time-varying gain matrix $\boldsymbol{L}$ so that we can make a probabilistic statement about the convergence of $\hat{\boldsymbol{x}}$ to $\boldsymbol{x}$.

C. Stochastically Stable G-Invariant Observer

We now aim to choose the gain matrix $\boldsymbol{L}$ such that the stochastic pre-observer given by Eqs. (28) and (29) is a stochastic *observer*. That is, we seek sufficient conditions for which a probabilistic statement of stability can be made about the zero-error manifold $\mathcal{Z}$. Since the sources of noise in Eq. (9) do not vanish on $\mathcal{Z}$, we must consider notions of stochastic stability for systems with *non-vanishing noise*.

1. Noise-to-State Stability

The SDE (16) with initial condition $\boldsymbol{x}(0,\omega)=\boldsymbol{x}_0$ (for almost all $\omega\in\Omega$) is *noise-to-state stable* (NSS) if for any $\epsilon\in(0,1]$ there exist a class-$\mathcal{K}$ function[§] α and a class-$\mathcal{KL}$ function β such that

$$\mathbb{P}\left\{\|\boldsymbol{x}(t)\|^p>\beta(\|\boldsymbol{x}_0\|,t)+\alpha(\|\boldsymbol{\sigma}\|)\right\}\leq\epsilon \quad (39)$$

for some integer $p>0$. The system is *pth moment noise-to-state stable* if there exist a class-$\mathcal{K}$ function α and a class-$\mathcal{KL}$ function β such that

$$\mathbb{E}\left\{\|\boldsymbol{x}(t)\|^p\right\}\leq\beta(\|\boldsymbol{x}_0\|,t)+\alpha(\|\boldsymbol{\sigma}\|) \quad (40)$$

where $\mathbb{E}\{X(t,\omega)\}=\int_\Omega X(t,\omega)\mathrm{d}\mathbb{P}(\omega)$ is the expected value of a random process X.

Sufficient conditions for NSS are given in [30], which we restate as follows.

Lemma 2 (Corollary 3.9 in [30])**.** *If there exist an integer $p>0$, a C^2-continuous Lyapunov function $V(\boldsymbol{x})$, a continuous positive definite function $W(\boldsymbol{x})$, class $\mathcal{K}_\infty$ functions α_1, α_2, and a class-$\mathcal{K}$ function ρ such that for all $\boldsymbol{x}\in\mathbb{R}^n$,*

$$\alpha_1(\|\boldsymbol{x}\|^p)\leq V(\boldsymbol{x})\leq\alpha_2(\|\boldsymbol{x}\|^p) \quad (41)$$
$$\mathscr{L}V(\boldsymbol{x})\leq -W(\boldsymbol{x})+\rho(\|\boldsymbol{\sigma}\|_{\mathrm{F}}) \quad (42)$$

where

$$V(\boldsymbol{x})\leq\alpha_3(W(\boldsymbol{x})) \quad (43)$$

for some concave class-$\mathcal{K}_\infty$ function α_3, then the system is noise-to-state stable in probability. Here, $\|\cdot\|_{\mathrm{F}}$ denotes the Frobenius norm. Specifically, for any $\epsilon\in(0,1]$,

$$\mathbb{P}\left\{\|\boldsymbol{x}(t)\|^p>\alpha_1^{-1}\left(\tfrac{2}{\epsilon}\mu\left(\alpha_2(\|\boldsymbol{x}_0\|^p),t\right)\right)+\alpha_1^{-1}\left(\tfrac{2}{\epsilon}\alpha_3\left(2\rho(\|\boldsymbol{\sigma}\|_{\mathrm{F}})\right)\right)\right\}\leq\epsilon \quad (44)$$

where the class-$\mathcal{KL}$ function $\mu(a,\tau)$ is defined by the solution to

$$\frac{\mathrm{d}y}{\mathrm{d}\tau}=-\frac{1}{2}\alpha_3^{-1}(y(\tau)),\quad y(0)=a \quad (45)$$

Furthermore, if α_1 is convex, then the system is pth moment noise-to-state stable in probability such that

$$\mathbb{E}\left\{\|\boldsymbol{x}(t)\|^p\right\}\leq\alpha_1^{-1}\left(2\mu\left(\alpha_2(\|\boldsymbol{x}_0\|^p),t\right)\right)+\alpha_1^{-1}\left(2\alpha_3\left(2\rho(\|\boldsymbol{\sigma}\|_{\mathrm{F}})\right)\right) \quad (46)$$

The convexity conditions in Lemma 2 are not required in Lyapunov stability theorems for deterministic systems [41]. They are needed here to leverage *Jensen's inequality*, where any convex function α of a random variable X satisfies $\alpha(\mathbb{E}\{X\})\leq\mathbb{E}\{\alpha(X)\}$ [42, Ch. 3]. See [30] for details on how this property applies to Lemma 2.

[§] See [41, Ch. 3] for the definitions of these comparison functions and properties of the $\mathcal{K}$ and $\mathcal{KL}$ function spaces.

2. Noise-to-State Stable Wind Observer

Now, we aim to select error coordinates whose origin is proven noise-to-state stable using Lemma 2. Like the deterministic case [40], consider the *invariant error coordinates*

$$\boldsymbol{\eta}(\boldsymbol{z},\boldsymbol{x},\boldsymbol{y}) = \boldsymbol{\varphi}_{\gamma(\boldsymbol{y})}(\boldsymbol{z}) + \boldsymbol{\ell}(\boldsymbol{\varrho}_{\gamma(\boldsymbol{y})}(\boldsymbol{y})) - \boldsymbol{\varphi}_{\gamma(\boldsymbol{y})}(\boldsymbol{x}) \tag{47}$$

They are invariant in the sense that $\boldsymbol{\eta} : \mathbb{R}^n \times \mathcal{X} \times \mathcal{Y} \to \mathcal{X}$ is an invariant map. They are valid error coordinates because $\boldsymbol{\eta} = \mathbf{0}$ if and only if $(\boldsymbol{z},\boldsymbol{x},\boldsymbol{y}) \in \mathcal{Z}$, the zero-error manifold prescribed in Eq. (31). Expanding Eq. (47), we have

$$\boldsymbol{\eta}_{v_{\mathrm{r}}} = \boldsymbol{z}_{v_{\mathrm{r}}} + \boldsymbol{L}^q_{v_{\mathrm{r}}}\boldsymbol{R}^{\mathsf{T}}_{\mathrm{IB}}\boldsymbol{q} + \boldsymbol{L}^\omega_{v_{\mathrm{r}}}\boldsymbol{\omega} - \boldsymbol{v}_{\mathrm{r}} \tag{48a}$$

$$\boldsymbol{\eta}_w = \boldsymbol{R}^{\mathsf{T}}_{\mathrm{IB}}\boldsymbol{z}_w + \boldsymbol{L}^q_w\boldsymbol{R}^{\mathsf{T}}_{\mathrm{IB}}\boldsymbol{q} + \boldsymbol{L}^\omega_w\boldsymbol{\omega} - \boldsymbol{R}^{\mathsf{T}}_{\mathrm{IB}}\boldsymbol{w} \tag{48b}$$

Using $\boldsymbol{\alpha}$ from Eq. (37), the application of Itô's rule to $\boldsymbol{\eta}$ yields the *invariant error SDE*

$$\mathrm{d}\boldsymbol{\eta}_{v_{\mathrm{r}}} = \big(-\boldsymbol{S}(\boldsymbol{\omega})\boldsymbol{\eta}_{v_{\mathrm{r}}} + \tfrac{1}{m}\boldsymbol{F}_v\boldsymbol{\eta}_{v_{\mathrm{r}}} - \boldsymbol{L}^q_{v_{\mathrm{r}}}(\boldsymbol{\eta}_{v_{\mathrm{r}}} + \boldsymbol{\eta}_w) - \boldsymbol{L}^\omega_{v_{\mathrm{r}}}\boldsymbol{I}^{-1}\boldsymbol{M}_v\boldsymbol{\eta}_{v_{\mathrm{r}}}\big)\,\mathrm{d}t + \begin{bmatrix}\boldsymbol{R}^{\mathsf{T}}_{\mathrm{IB}} & \boldsymbol{L}^\omega_{v_{\mathrm{r}}} & -\mathbb{I}\end{bmatrix}\boldsymbol{\sigma}\mathrm{d}\boldsymbol{\mathcal{W}} \tag{49a}$$

$$\mathrm{d}\boldsymbol{\eta}_w = \big(-\boldsymbol{L}^q_w(\boldsymbol{\eta}_{v_{\mathrm{r}}} + \boldsymbol{\eta}_w) - \boldsymbol{L}^\omega_w\boldsymbol{I}^{-1}\boldsymbol{M}_v\boldsymbol{\eta}_{v_{\mathrm{r}}} - \boldsymbol{S}(\boldsymbol{\omega})\boldsymbol{\eta}_w\big)\,\mathrm{d}t + \begin{bmatrix}-\boldsymbol{R}^{\mathsf{T}}_{\mathrm{IB}} & \boldsymbol{L}^\omega_w & \mathbf{0}\end{bmatrix}\boldsymbol{\sigma}\mathrm{d}\boldsymbol{\mathcal{W}} \tag{49b}$$

which we may compactly write as

$$\mathrm{d}\boldsymbol{\eta} = \big(\boldsymbol{A}(t) - \boldsymbol{L}\boldsymbol{C}(t)\big)\boldsymbol{\eta}\,\mathrm{d}t + \big(\boldsymbol{B}(t) - \boldsymbol{L}\boldsymbol{D}\big)\boldsymbol{\sigma}\mathrm{d}\boldsymbol{\mathcal{W}} \tag{50}$$

where

$$\begin{aligned}
\boldsymbol{A}(t) &= \begin{bmatrix}-\boldsymbol{S}(\boldsymbol{\omega}(t)) + \boldsymbol{F}_v(t)/m & \mathbf{0}\\ \mathbf{0} & -\boldsymbol{S}(\boldsymbol{\omega}(t))\end{bmatrix} & \boldsymbol{C}(t) &= \begin{bmatrix}\mathbb{I} & \mathbb{I}\\ \boldsymbol{I}^{-1}\boldsymbol{M}_v(t) & \mathbf{0}\end{bmatrix}\\
\boldsymbol{B}(t) &= \begin{bmatrix}\boldsymbol{R}^{\mathsf{T}}_{\mathrm{IB}}(t) & \mathbf{0} & -\mathbb{I}\\ -\boldsymbol{R}^{\mathsf{T}}_{\mathrm{IB}}(t) & \mathbf{0} & \mathbf{0}\end{bmatrix} & \boldsymbol{D} &= \begin{bmatrix}\mathbf{0} & \mathbf{0} & \mathbf{0}\\ \mathbf{0} & -\mathbb{I} & \mathbf{0}\end{bmatrix}
\end{aligned} \tag{51}$$

Since $\boldsymbol{y}$ is a known signal, the stabilization of the invariant error SDE (50) is reduced to LTV observer design for the fictitious linear input-output SDE

$$\begin{aligned}
\mathrm{d}\boldsymbol{\xi} &= \boldsymbol{A}(t)\boldsymbol{\xi}\mathrm{d}t + \boldsymbol{B}(t)\boldsymbol{\sigma}\mathrm{d}\boldsymbol{\mathcal{W}}\\
\mathrm{d}\boldsymbol{\zeta} &= \boldsymbol{C}(t)\boldsymbol{\xi}\mathrm{d}t + \boldsymbol{D}\boldsymbol{\sigma}\mathrm{d}\boldsymbol{\mathcal{W}}
\end{aligned} \tag{52}$$

where ζ is the *observation process* whose derivative is the typical output considered in the linear filtering problem. The remarkable result here is that the solution to the gain design problem is *almost* the standard Kalman-Bucy filter. The only barrier is that $\boldsymbol{D}$ has rows of zeros, meaning some of the outputs are noise-free. Since we are constrained to the closed loop error dynamics (50) and cannot consider more general formulations (e.g., taking derivatives of the noise-free output [43]), we consider a *blended approach* to tuning which does not necessarily produce the minimum variance estimate, but still will be shown to be noise-to-state stable. First, notice the structures of $\boldsymbol{B}$ and $\boldsymbol{D}$ imply that the components of $\mathrm{d}\boldsymbol{\mathcal{W}}$ entering the $\mathrm{d}\boldsymbol{\xi}$ and $\mathrm{d}\boldsymbol{\zeta}$ equations are distinct; that is, the "process noise" and "measurement noise" in Eq. (52) are uncorrelated. Accordingly, let

$$\bar{\boldsymbol{B}} = \begin{bmatrix}\boldsymbol{R}^{\mathsf{T}}_{\mathrm{IB}} & -\mathbb{I}\\ -\boldsymbol{R}^{\mathsf{T}}_{\mathrm{IB}} & \mathbf{0}\end{bmatrix}, \qquad \bar{\boldsymbol{D}} = \begin{bmatrix}\mathbf{0}\\ -\mathbb{I}\end{bmatrix} \tag{53}$$

reflect the non-zero input channels of $\boldsymbol{B}$ and $\boldsymbol{D}$, respectively. To circumvent the rank deficiency of $\bar{\boldsymbol{D}}\bar{\boldsymbol{D}}^{\mathsf{T}}$, define

$$\bar{\boldsymbol{R}} = \begin{bmatrix}\bar{\boldsymbol{D}}\boldsymbol{\sigma}_M & \tilde{\boldsymbol{D}}\end{bmatrix}\begin{bmatrix}\bar{\boldsymbol{D}}\boldsymbol{\sigma}_M & \tilde{\boldsymbol{D}}\end{bmatrix}^{\mathsf{T}} \tag{54}$$

where $\tilde{\boldsymbol{D}} \in \mathbb{R}^{6\times 3}$ is a tuning parameter that ensures $\bar{\boldsymbol{R}}$ is invertible. The positive definite matrix $\bar{\boldsymbol{R}}$ can be thought of as the power spectral density of an augmented measurement noise vector in Eq. (52). For the process noise, we have

$$\bar{\boldsymbol{Q}} = \mathbf{diag}(\boldsymbol{\sigma}_w\boldsymbol{\sigma}_w^{\mathsf{T}}, \boldsymbol{\sigma}_F\boldsymbol{\sigma}_F^{\mathsf{T}}) \tag{55}$$

Since $\boldsymbol{A}(t)$ and $\boldsymbol{B}(t)$ are bounded, uniform observability of the pair $(\boldsymbol{A}(t), \boldsymbol{C}(t))$ is a sufficient condition [44] for the existence of a bounded solution $\boldsymbol{P}(t)$ to the differential Riccati equation

$$\dot{\boldsymbol{P}}(t) = \boldsymbol{A}(t)\boldsymbol{P}(t) + \boldsymbol{P}(t)\boldsymbol{A}(t)^{\mathsf{T}} - \boldsymbol{P}(t)\boldsymbol{C}(t)^{\mathsf{T}}\bar{\boldsymbol{R}}^{-1}\boldsymbol{C}(t)\boldsymbol{P}(t) + \bar{\boldsymbol{B}}(t)\bar{\boldsymbol{Q}}\bar{\boldsymbol{B}}(t)^{\mathsf{T}} \tag{56}$$

Assuming uniform observability, let the observer gain matrix satisfy

$$\boldsymbol{L}(t) = \boldsymbol{P}(t)\boldsymbol{C}(t)^{\mathsf{T}}\bar{\boldsymbol{R}}^{-1} \tag{57}$$

Remark 2. *Requiring observability of $(\boldsymbol{A}(t), \boldsymbol{C}(t))$ is not overly restrictive. Most nonlinear aerodynamic models for both fixed-wing and multirotor aircraft satisfy this observability requirement. For example, constructing $\boldsymbol{F}_v$ and $\boldsymbol{M}_v$ from the large-domain fixed-wing and multirotor models given in [45] and [46], respectively, both yield observability. The theoretical results are demonstrated in simulations of a multirotor aircraft in the Section V.*

Finally, we apply a time-varying version of Lemma 2 to prove noise-to-state stability and obtain probabilistic guarantees on the stability of the invariant error system (50). Consider the Lyapunov function

$$V(t, \boldsymbol{\eta}) = \boldsymbol{\eta}^{\mathsf{T}} \boldsymbol{P}^{-1}(t) \boldsymbol{\eta} \tag{58}$$

where $\boldsymbol{P}(t)$ satisfies Eq. (56). Consider the time interval $\mathbb{T} = [0, T)$ and let

$$k_1 = \inf_{t \in \mathbb{T}} \lambda_{\min}(\boldsymbol{P}^{-1}(t)), \qquad k_2 = \sup_{t \in \mathbb{T}} \lambda_{\max}(\boldsymbol{P}^{-1}(t)) \tag{59}$$

Then by the Rayleigh-Ritz inequality,

$$k_1 \|\boldsymbol{\eta}\|^2 \leq V(t, \boldsymbol{\eta}) \leq k_2 \|\boldsymbol{\eta}\|^2 \tag{60}$$

to satisfy Eq. (41). The expected rate-of-change of V is

$$\begin{aligned} \frac{\partial V}{\partial t} + \mathscr{L} V = -\boldsymbol{\eta}^{\mathsf{T}} \Big(\boldsymbol{C}^{\mathsf{T}}(t) \bar{\boldsymbol{R}}^{-1} \boldsymbol{C}(t) + \boldsymbol{P}^{-1}(t) \bar{\boldsymbol{B}}(t) \bar{\boldsymbol{Q}} \bar{\boldsymbol{B}}^{\mathsf{T}}(t) \boldsymbol{P}^{-1}(t) \Big) \boldsymbol{\eta} \\ + \frac{1}{2} \operatorname{Tr} \Big(\boldsymbol{\sigma}^{\mathsf{T}} \big(\boldsymbol{B}(t) - \boldsymbol{L}\boldsymbol{D} \big)^{\mathsf{T}} \boldsymbol{P}^{-1} \big(\boldsymbol{B}(t) - \boldsymbol{L}\boldsymbol{D} \big) \boldsymbol{\sigma} \Big) \end{aligned} \tag{61}$$

Let

$$k_3 = \inf_{t \in \mathbb{T}} \lambda_{\min} \Big(\boldsymbol{C}^{\mathsf{T}}(t) \bar{\boldsymbol{R}}^{-1} \boldsymbol{C}(t) + \boldsymbol{P}^{-1}(t) \bar{\boldsymbol{B}}(t) \bar{\boldsymbol{Q}} \bar{\boldsymbol{B}}^{\mathsf{T}}(t) \boldsymbol{P}^{-1}(t) \Big) \tag{62}$$

$$k_4 = \sup_{t \in \mathbb{T}} \operatorname{Tr} \Big(\big(\boldsymbol{B}(t) - \boldsymbol{L}\boldsymbol{D} \big)^{\mathsf{T}} \boldsymbol{P}^{-1}(t) \big(\boldsymbol{B}(t) - \boldsymbol{L}\boldsymbol{D} \big) \Big) \tag{63}$$

By the definition and sub-multiplicative property of the Frobenius norm,

$$\frac{\partial V}{\partial t} + \mathscr{L} V \leq -k_3 \|\boldsymbol{\eta}\|^2 + \frac{1}{2} k_4 \|\boldsymbol{\sigma}\|_{\mathrm{F}}^2 \tag{64}$$

to satisfy Eq. (42). Recalling the positive integer p represents the order of a particular statistical moment of interest, the comparison functions in Eqs. (41)–(43) of Lemma 2 are

$$\alpha_1(a) = \begin{cases} k_1 a^2, & p = 1 \\ k_1 a, & p = 2 \end{cases}, \quad \alpha_2(a) = \begin{cases} k_2 a^2, & p = 1 \\ k_2 a, & p = 2 \end{cases}, \quad \alpha_3(a) = \frac{k_2}{k_3} a, \quad \rho(a) = \frac{1}{2} k_4 a^2 \tag{65}$$

which proves noise-to-state stability of the invariant error system (50). Furthermore, since α_1 is convex, the error system is also pth moment noise-to-state stable. Because α_3 is linear, the class-$\mathcal{KL}$ function μ is simply

$$\mu(a, \tau) = a \exp\left(-\frac{1}{2} \frac{k_3}{k_2} \tau \right) \tag{66}$$

Therefore, the invariant error system (50) is *uniformly noise-to-state stable* with guarantees that

$$\mathbb{P} \left\{ \|\boldsymbol{\eta}(t)\| > \sqrt{\frac{2}{\epsilon} \frac{k_2}{k_1}} \|\boldsymbol{\eta}_0\| \sqrt{\exp\left(-\frac{1}{2} \frac{k_3}{k_2} t \right)} + \sqrt{\frac{2}{\epsilon} \frac{k_2 k_4}{k_1 k_3}} \|\boldsymbol{\sigma}\|_{\mathrm{F}} \right\} \leq \epsilon \tag{67a}$$

$$\mathbb{E} \left\{ \|\boldsymbol{\eta}(t)\| \right\} \leq \sqrt{2 \frac{k_2}{k_1}} \|\boldsymbol{\eta}_0\| \sqrt{\exp\left(-\frac{1}{2} \frac{k_3}{k_2} t \right)} + \sqrt{2 \frac{k_2 k_4}{k_1 k_3}} \|\boldsymbol{\sigma}\|_{\mathrm{F}} \tag{67b}$$

$$\mathbb{P} \left\{ \|\boldsymbol{\eta}(t)\|^2 > \frac{2}{\epsilon} \frac{k_2}{k_1} \|\boldsymbol{\eta}_0\|^2 \exp\left(-\frac{1}{2} \frac{k_3}{k_2} t \right) + \frac{2}{\epsilon} \frac{k_2 k_4}{k_1 k_3} \|\boldsymbol{\sigma}\|_{\mathrm{F}}^2 \right\} \leq \epsilon \tag{68a}$$

$$\mathbb{E} \left\{ \|\boldsymbol{\eta}(t)\|^2 \right\} \leq 2 \frac{k_2}{k_1} \|\boldsymbol{\eta}_0\|^2 \exp\left(-\frac{1}{2} \frac{k_3}{k_2} t \right) + 2 \frac{k_2 k_4}{k_1 k_3} \|\boldsymbol{\sigma}\|_{\mathrm{F}}^2 \tag{68b}$$

The probabilistic convergence guarantees in Eqs. (67) and (68) can be extremely useful. Equations (67a) and (68a) may be used to provide confidence intervals on bounds of the exponential convergence. For example, one can conclude there is a 1% chance that $\|\boldsymbol{\eta}(t)\|$ ever exceeds

$$10\sqrt{2\frac{k_2}{k_1}}\|\boldsymbol{\eta}_0\|\sqrt{\exp\left(-\frac{1}{2}\frac{k_3}{k_2}t\right)}+10\sqrt{2\frac{k_2k_4}{k_1k_3}}\|\boldsymbol{\sigma}\|_{\mathrm{F}}$$

From another perspective, one may wish to simply know bounds on the steady-state statistics. That is,

$$\mathbb{E}\left\{\|\boldsymbol{\eta}(\infty)\|\right\}\leq\sqrt{2\frac{k_2k_4}{k_1k_3}}\|\boldsymbol{\sigma}\|_{\mathrm{F}}\quad\text{and}\quad\mathbb{E}\left\{\|\boldsymbol{\eta}(\infty)\|^2\right\}\leq2\frac{k_2k_4}{k_1k_3}\|\boldsymbol{\sigma}\|_{\mathrm{F}}^2$$

3. Alternative Tuning Approach

Altogether, the noise-to-state stability guarantees in Eqs. (67) and (68) are a principled quantification of wind estimation performance in the presence of both modeling error and turbulence. However, these bounds may be overly conservative, especially in scenarios where $k_1 \ll k_2$. An alternative approach is to consider $\bar{\boldsymbol{Q}}$ and $\bar{\boldsymbol{R}}$ as tuning parameters rather than noise power spectral densities. In this case, it is beneficial to choose $\bar{\boldsymbol{Q}}$ and $\bar{\boldsymbol{R}}$ to optimize the noise-to-state stability bounds. In contrast to the *blended approach* described earlier, we call this the *optimal bounds approach* to tuning the observer. Examining Eqs. (67) and (68), we let

$$J_{\mathrm{init}}=\frac{k_2}{k_1},\quad J_{\mathrm{rate}}=\frac{k_2}{k_3},\quad\text{and}\quad J_{\mathrm{ss}}=\frac{k_4}{k_3}\tag{69}$$

which are proportional to the guaranteed initial error, inverse of the convergence rate, and steady-state error, respectively. This observation motivates choosing the penalty matrices in the design of the observer gain matrix to minimize the cost function

$$J=J_{\mathrm{init}}+\kappa_1J_{\mathrm{rate}}+\kappa_2J_{\mathrm{ss}}\tag{70}$$

where κ_1 and κ_2 are non-negative weighting parameters. To simplify this optimization, let $\boldsymbol{A}_0$, $\boldsymbol{B}_0$, and $\boldsymbol{C}_0$ be the constant matrices defined by evaluating Eq. (51) at some nominal flight condition. Then, let $\boldsymbol{L}_0=\boldsymbol{P}_0\boldsymbol{C}_0^{\mathsf{T}}\bar{\boldsymbol{R}}^{-1}$ where $\boldsymbol{P}_0$ satisfies the algebraic Riccati equation $\boldsymbol{A}_0\boldsymbol{P}_0+\boldsymbol{P}_0\boldsymbol{A}_0^{\mathsf{T}}-\boldsymbol{P}_0\boldsymbol{C}_0^{\mathsf{T}}\bar{\boldsymbol{R}}^{-1}\boldsymbol{C}_0\boldsymbol{P}_0+\bar{\boldsymbol{B}}_0\bar{\boldsymbol{Q}}\bar{\boldsymbol{B}}_0^{\mathsf{T}}=\boldsymbol{0}$. Using a constrained optimization solver, J can be minimized over $\bar{\boldsymbol{Q}}$ and $\bar{\boldsymbol{R}}$ while constraining $\bar{\boldsymbol{Q}}$ and $\bar{\boldsymbol{R}}$ to be positive definite and norm bounded (e.g., $\|\bar{\boldsymbol{Q}}\|_{\mathrm{F}}\leq100$ and $\|\bar{\boldsymbol{R}}\|_{\mathrm{F}}\leq100$). A comparison between the tuning approaches of Sections IV.C.2 and IV.C.3 will be made through numerical simulation in the following section.

V. Simulation Results

A. Simulation Scenario

The stochastic symmetry-preserving reduced-order wind observer was implemented on simulated flight data for the small quadrotor UAV considered in [46] whose geometry is shown in Figure 3. Neglecting velocity-dependent inflow

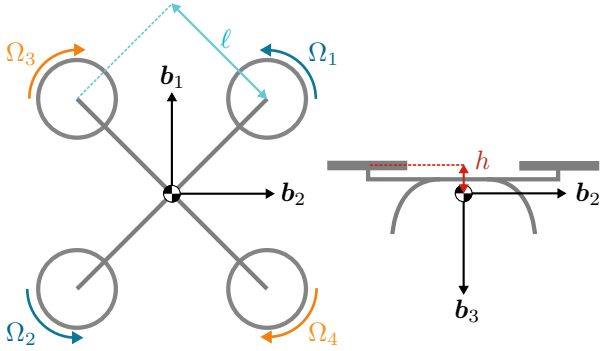

Fig. 3 Quadrotor geometry.

effects, airframe drag, and motor inertia for simplicity, we consider the following nonlinear aerodynamic model.

$$F_x = \rho\pi R^2 N_{\mathrm{r}} u_{\mathrm{r}} \left(-C_{H_{\mu_x}} R\delta t - C_{H_{\mu_0,\mu_x}} \nu_0 - C_{H_{\mu_x,\mu_z}} w_{\mathrm{r}}\right) \tag{71a}$$

$$F_y = \rho\pi R^2 N_{\mathrm{r}} v_{\mathrm{r}} \left(-C_{H_{\mu_x}} R\delta t - C_{H_{\mu_0,\mu_x}} \nu_0 - C_{H_{\mu_x,\mu_z}} w_{\mathrm{r}}\right) \tag{71b}$$

$$F_z = \rho\pi R^2 \Big(- C_{T_0} R^2 N_{\mathrm{r}} \delta^2 t + C_{T_{\mu_0}} R N_{\mathrm{r}} \nu_0 \delta t + C_{T_{\mu_z}} R\big(N_{\mathrm{r}} w_{\mathrm{r}} \delta t - p\delta a - q\delta e\big) - C_{T_{\mu_x^2}} N_{\mathrm{r}} (u_{\mathrm{r}}^2 + v_{\mathrm{r}}^2)\Big) \tag{71c}$$

$$\begin{aligned} M_x = \rho\pi R^2 \Big(& - C_{R_{\mu_x}} R^2 u_{\mathrm{r}} \delta r + C_{T_0} R^2 \delta^2 a - C_{T_{\mu_0}} R \nu_0 \delta a - C_{T_{\mu_z}} R\big(w_{\mathrm{r}} \delta a - \tfrac{1}{2}\ell^2 (N_{\mathrm{r}} p \delta t + q\delta r)\big) \\ & - C_{H_{\mu_x}} R N_{\mathrm{r}} h v_{\mathrm{r}} \delta t - C_{H_{\mu_0,\mu_x}} N_{\mathrm{r}} h v_{\mathrm{r}} \nu_0 - C_{H_{\mu_x,\mu_z}} N_{\mathrm{r}} h v_{\mathrm{r}} w_{\mathrm{r}}\Big) \end{aligned} \tag{71d}$$

$$\begin{aligned} M_y = \rho\pi R^2 \Big(& - C_{R_{\mu_x}} R^2 v_{\mathrm{r}} \delta r + C_{T_0} R^2 \delta^2 e - C_{T_{\mu_0}} R \nu_0 \delta e - C_{T_{\mu_z}} R\big(w_{\mathrm{r}} \delta e - \tfrac{1}{2}\ell^2 (N_{\mathrm{r}} q \delta t + p\delta r)\big) \\ & + C_{H_{\mu_x}} R N_{\mathrm{r}} h u_{\mathrm{r}} \delta t + C_{H_{\mu_0,\mu_x}} N_{\mathrm{r}} h u_{\mathrm{r}} \nu_0 + C_{H_{\mu_x,\mu_z}} N_{\mathrm{r}} h u_{\mathrm{r}} w_{\mathrm{r}}\Big) \end{aligned} \tag{71e}$$

$$\begin{aligned} M_z = \rho\pi R^2 \Big(& C_{Q_0} R^3 \delta^2 r + C_{Q_{\mu_0}} R^2 \nu_0 \delta r + C_{Q_{\mu_z}} R^2 \big(w_{\mathrm{r}} \delta r - p\delta e - q\delta a\big) - C_{Q_{\mu_z^2}} R N_{\mathrm{r}} \ell^2 pq \\ & - C_{H_{\mu_x}} R(u_{\mathrm{r}} \delta a + v_{\mathrm{r}} \delta e) + \tfrac{1}{2} C_{H_{\mu_x,\mu_z}} N_{\mathrm{r}} \ell^2 (u_{\mathrm{r}} p + v_{\mathrm{r}} q)\Big) \end{aligned} \tag{71f}$$

Here, ρ is the air density, R is the rotor radius, $N_{\mathrm{r}} = 4$ is the number of rotors, ν_0 is the rotor inflow velocity in hover, ℓ is the arm length, h is the height of the rotor disc above the vehicle center of gravity, and $\boldsymbol{\delta} = (\delta t, \delta a, \delta e, \delta r)$, $\boldsymbol{\delta}^2 = (\delta^2 t, \delta^2 a, \delta^2 e, \delta^2 r)$ are virtual actuators satisfying

$$\begin{bmatrix} \delta t \\ \delta a \\ \delta e \\ \delta r \end{bmatrix} = \mathbf{M_{ix}} \begin{bmatrix} \Omega_1 \\ \Omega_2 \\ \vdots \\ \Omega_{N_{\mathrm{r}}} \end{bmatrix}, \qquad \begin{bmatrix} \delta^2 t \\ \delta^2 a \\ \delta^2 e \\ \delta^2 r \end{bmatrix} = \mathbf{M_{ix}} \begin{bmatrix} \Omega_1^2 \\ \Omega_2^2 \\ \vdots \\ \Omega_{N_{\mathrm{r}}}^2 \end{bmatrix} \tag{72}$$

for motor speeds $\Omega_1, \ldots, \Omega_{N_{\mathrm{r}}}$. The mixing matrix $\mathbf{M_{ix}}$ is determined by the geometry of the aircraft (Figure 3) and is given for the quadrotor in consideration as follows:

$$\mathbf{M_{ix}} = \begin{bmatrix} \frac{1}{4} & \frac{1}{4} & \frac{1}{4} & \frac{1}{4} \\ -\ell\frac{\sqrt{2}}{2} & +\ell\frac{\sqrt{2}}{2} & +\ell\frac{\sqrt{2}}{2} & -\ell\frac{\sqrt{2}}{2} \\ +\ell\frac{\sqrt{2}}{2} & -\ell\frac{\sqrt{2}}{2} & +\ell\frac{\sqrt{2}}{2} & -\ell\frac{\sqrt{2}}{2} \\ +1 & +1 & -1 & -1 \end{bmatrix} \tag{73}$$

Note that $\boldsymbol{\delta}$ and $\boldsymbol{\delta}^2$ are not independent but rather are related through $\mathbf{M_{ix}}$. Therefore, we consider $\boldsymbol{\delta}$ to be the control input.

To demonstrate the theoretical performance guarantees, the stochastic aircraft dynamics and observer were simulated using the Euler-Maruyama scheme [47, Ch. 10] with all assumptions satisfied. That is, the aerodynamic force and moment satisfy Assumption 3 and the wind is Brownian motion to satisfy Assumption 1. For all simulations, the components of $\boldsymbol{\sigma}$ were

$$\boldsymbol{\sigma}_w = 0.5\,\mathbb{I}, \quad \boldsymbol{\sigma}_M = \mathbf{diag}(2.30, 2.21, 5.83) \times 10^{-2}, \quad \boldsymbol{\sigma}_F = \mathbf{diag}(3.55, 3.55, 1.77) \times 10^{-2}$$

For this ideal case, we decompose the nonlinear aerodynamic model in Eq. (71) according to Eq. (6) and evaluate the argument $\boldsymbol{v}_{\mathrm{r}}$ in $\boldsymbol{F}_0$, $\boldsymbol{F}_v$, etc. to a nominal value of zero. Note this only affects the few terms in Eq. (71) that are nonlinear in air-relative velocity. In all simulations, the components of the initial apparent wind velocity were $w_{\mathrm{N}} = 10$ m/s, $w_{\mathrm{E}} = -10$ m/s, and $w_{\mathrm{D}} = 0$ m/s.

To showcase the nonlinear stability guarantees and global nature of the observer, a large-amplitude multisine input excitation was injected on top of the feedback control signal (Figure 4a). The multisine was constructed with frequencies ranging from 0.01 to 1 Hz to effectively explore the state space as seen in Figure 4.

The observability condition mentioned in Remark 2 was verified for each simulated trajectory. The LTV observability Gramian $\boldsymbol{G}_o(t_0, t_f)$ was numerically constructed backwards in time from $t_f = 10$ to $t_0 = 0$. As shown in Figure 5 for the same simulation as Figure 4, the minimum eigenvalue of the observability Gramian is bounded away from

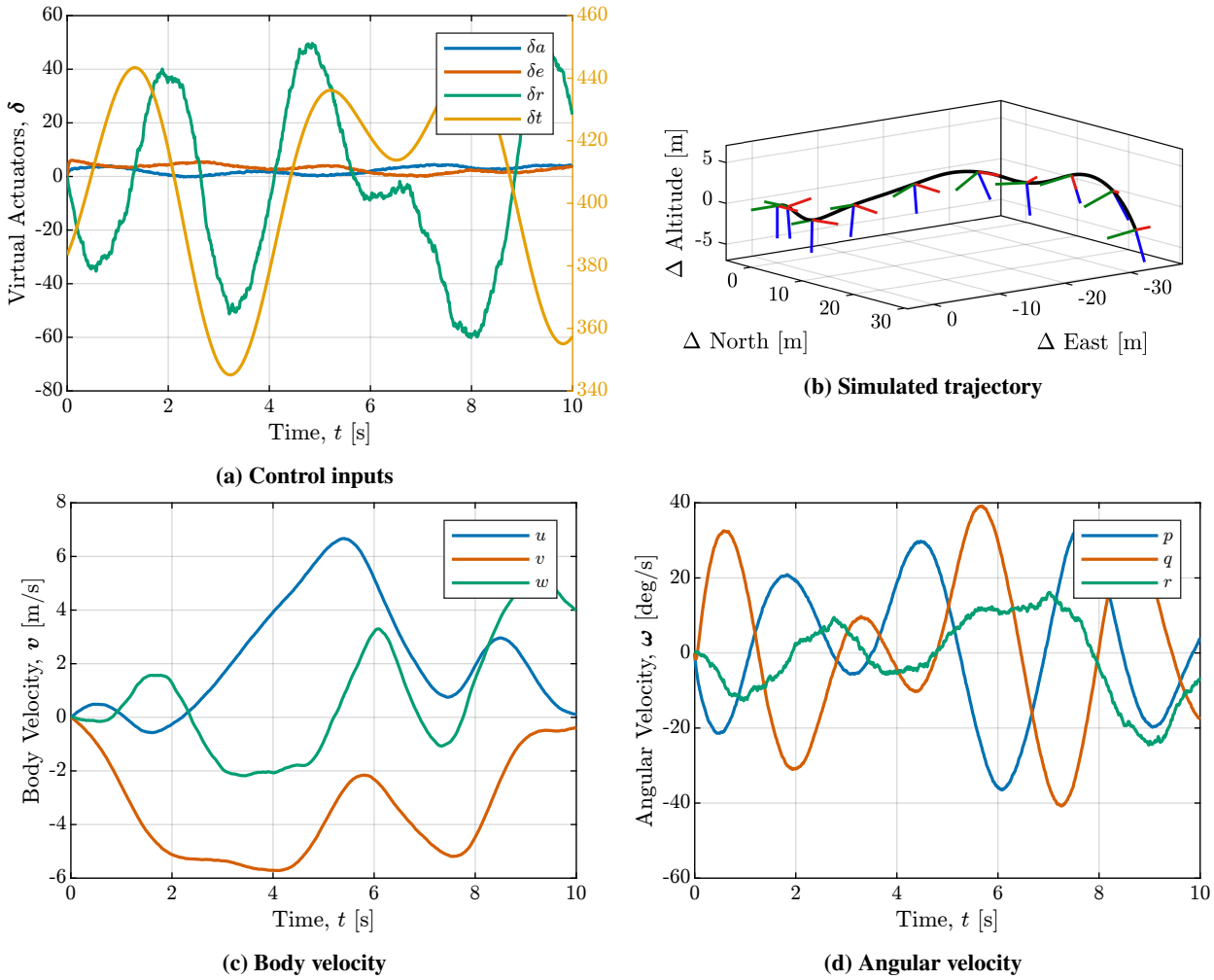

(a) Control inputs

(b) Simulated trajectory

(c) Body velocity

(d) Angular velocity

Fig. 4 Sample paths of the aircraft state and inputs in turbulent wind.

zero backwards in time, implying observability of $(\boldsymbol{A}(t), \boldsymbol{C}(t))$ on $[t_0, 10]$ for any $t_0 \geq 0$ [48, Ch. 9]. Also shown in Figure 5 is the minimum eigenvalue of the observability Gramian for the nominal hover flight condition in zero wind, showing persistent maneuvering is not a requirement for this observer.

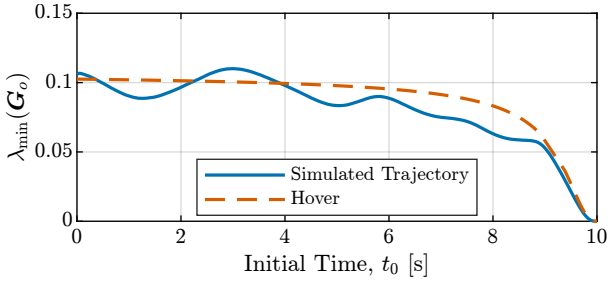

Fig. 5 Minimum eigenvalue of the LTV observability Gramian on the interval $[t_0, 10]$.

B. Blended Approach to Tuning

First, the blended tuning approach described in Section IV.C.2 was considered. The free tuning parameter $\tilde{\boldsymbol{D}}$ was chosen as $\tilde{\boldsymbol{D}} = [\mathbb{I}\ \ \mathbf{0}]^{\mathsf{T}} \times 10^{-3}$. To evaluate the conservatism of the noise-to-state stability guarantees, 1000 simulations of the stochastic aircraft dynamics and observer with initial estimate $\hat{\boldsymbol{x}} = \mathbf{0}$ were conducted to numerically approximate the probability density of $\|\boldsymbol{\eta}(t)\|$. The result of these simulations is shown in Figure 6, where we see exponential convergence to a stationary distribution within about one second. The computed mean $\mu(t) = \mathrm{E}\{\|\boldsymbol{\eta}(t)\|\}$ and standard

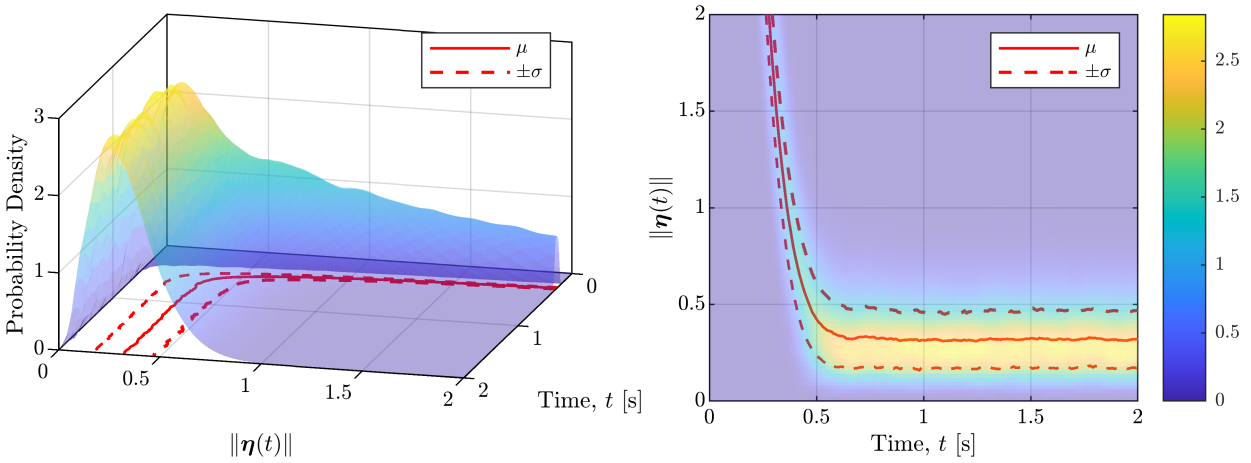

Fig. 6 Probability density of the error $\|\boldsymbol{\eta}(t)\|$ using the blended tuning approach.

deviation $\sigma(t) = \sqrt{\mathrm{E}\{(\|\boldsymbol{\eta}(t)\| - \mu(t))^2\}}$ are shown in red. For this tuning, the noise-to-state stability guarantees held across all simulations with

$$k_1 = 15.6, \quad k_2 = 5.9 \times 10^4, \quad k_3 = 240, \quad \text{and} \quad k_4 = 1.21 \times 10^5 \tag{74}$$

The corresponding bounds on the first and second moments of $\|\boldsymbol{\eta}(t)\|$ are shown in Figure 7 along with the moments computed from Monte-Carlo simulations. Clearly, these bounds are extremely conservative and thus not useful. Regardless, the representative time history in Figure 8 along with the Monte-Carlo results demonstrate the excellent

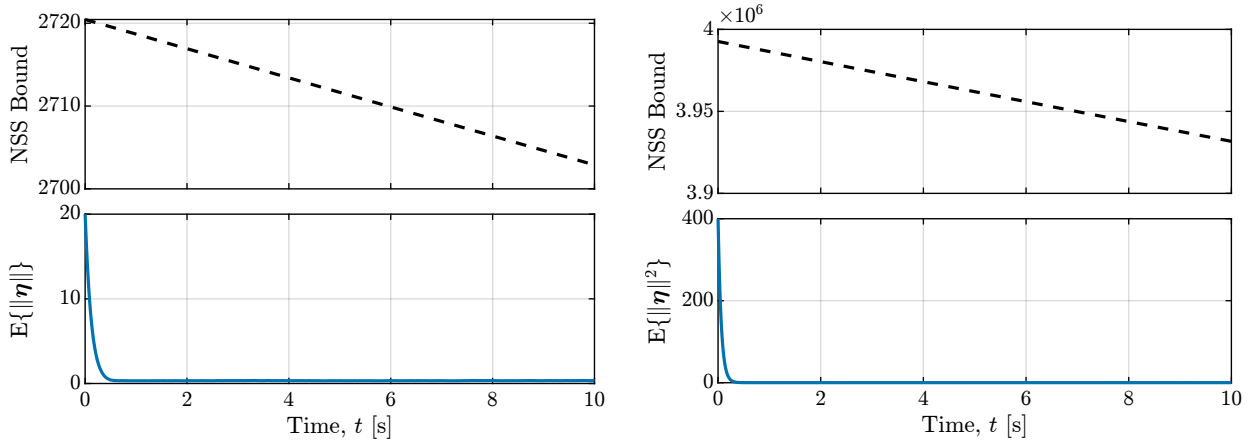

(a) First moment **(b) Second Moment**

Fig. 7 First and second moment noise-to-state stability guarantees for the blended tuning approach.

performance of the observer even though the statistical guarantees are too conservative to support it.

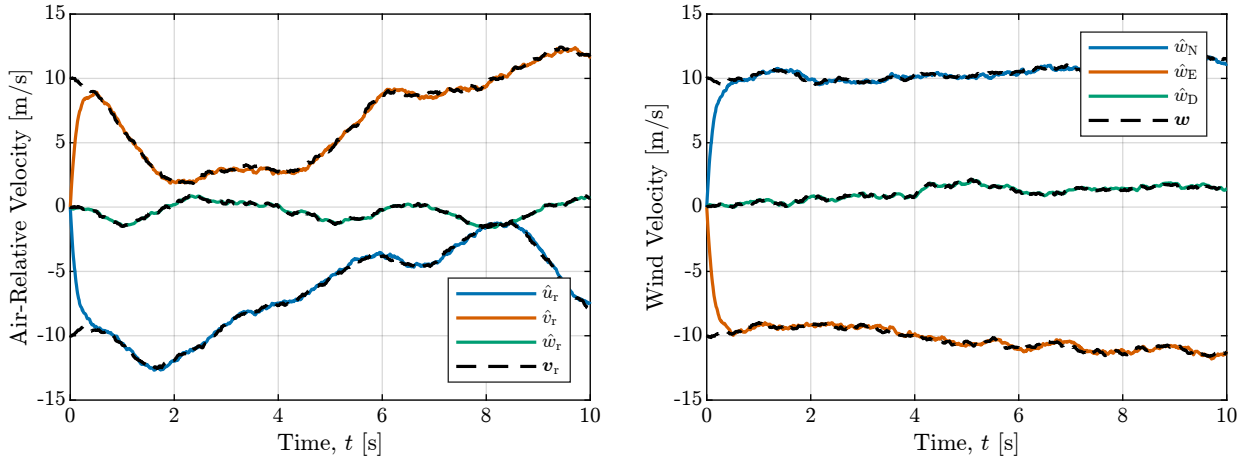

(a) Air-relative velocity **(b) Wind velocity**

Fig. 8 Sample time history of state estimates using the blended tuning approach.

C. Optimal Bounds Approach to Tuning

Next, we consider the alternative tuning approach described in Section IV.C.3 in which the aim is to minimize a weighted sum of the guaranteed initial error, inverse of the convergence rate, and steady-state error. With $\kappa_1 = 10$ and $\kappa_2 = 1$, the cost function J given in Eq. (70) was minimized to yield

$$\bar{\boldsymbol{Q}} = \begin{bmatrix} 13.60 & 0.65 & -0.28 & 22.98 & 1.76 & -0.71 \\ 0.65 & 15.71 & 0.75 & 1.90 & 29.06 & 0.45 \\ -0.28 & 0.75 & 18.86 & -0.24 & 1.27 & 15.66 \\ 22.98 & 1.90 & -0.24 & 46.92 & 4.82 & -1.51 \\ 1.76 & 29.06 & 1.27 & 4.82 & 63.07 & 0.68 \\ -0.71 & 0.45 & 15.66 & -1.51 & 0.68 & 91.99 \end{bmatrix}, \quad \bar{\boldsymbol{R}} = \begin{bmatrix} 16.79 & -2.15 & 0.02 & 0.44 & 3.17 & -0.02 \\ -2.15 & 8.91 & -0.18 & -1.78 & -0.39 & 0 \\ 0.02 & -0.18 & 4.08 & 0.04 & -0.01 & 0 \\ 0.44 & -1.78 & 0.04 & 1.06 & 0.08 & 0 \\ 3.17 & -0.39 & -0.01 & 0.08 & 1.25 & -0.01 \\ -0.02 & 0 & 0 & 0 & -0.01 & 52.79 \end{bmatrix}$$

Again, we perform 1000 simulations of the stochastic aircraft dynamics and observer to numerically approximate the probability density of $\|\boldsymbol{\eta}(t)\|$. These results are shown in Figure 9, where we see exponential convergence to a stationary distribution distinct from Figure 6. Note the difference in scale between Figures 6 and 9. For this tuning approach, the

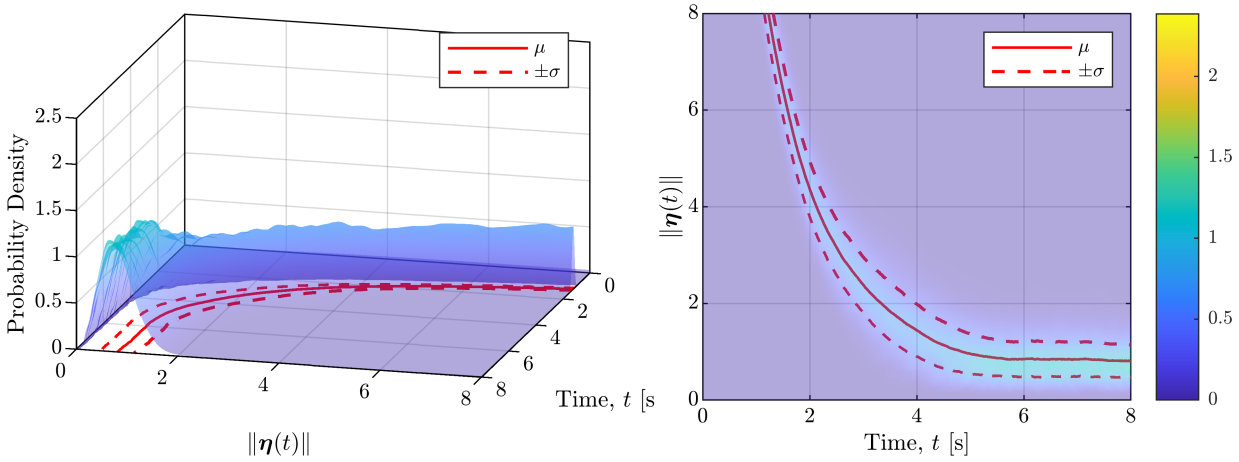

Fig. 9 Probability density of the error $\|\boldsymbol{\eta}(t)\|$ using the optimal bounds tuning approach.

noise-to-state stability guarantees held across all simulations with

$$k_1 = 0.06, \quad k_2 = 0.24, \quad k_3 = 0.14, \quad \text{and} \quad k_4 = 5.08 \tag{75}$$

The guarantees shown in Figure 10 are much less conservative than the previous tuning, but are still not a reflection of the Monte-Carlo results. Further, as seen in Figure 11, this tuning approach yields less conservative bounds at the

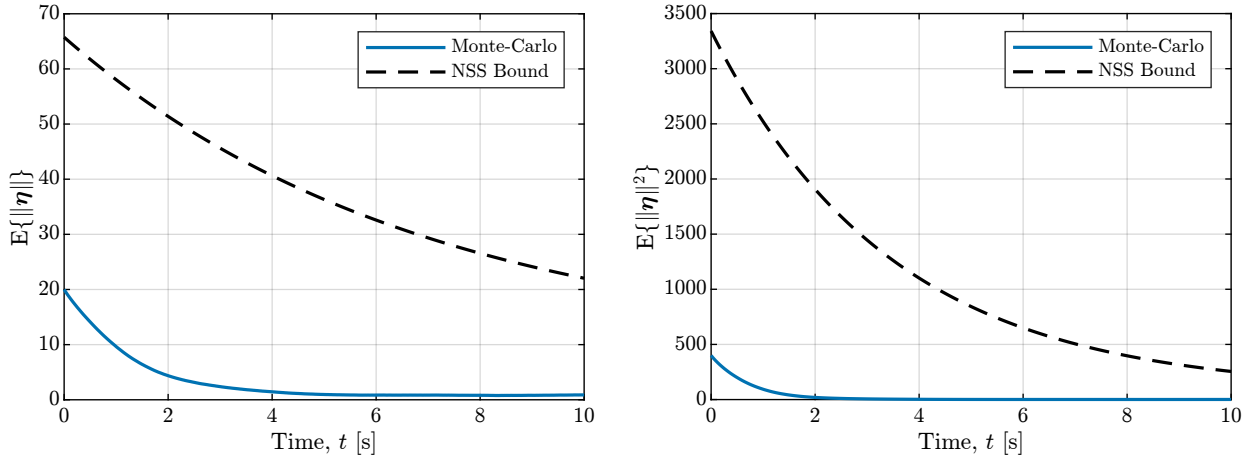

(a) First moment **(b) Second Moment**

Fig. 10 First and second moment noise-to-state stability guarantees for the optimal bounds tuning approach.

expense of performance. The convergence of the first and second moments of the estimate error is slower than in Figure 6. Similarly, the computed steady-state mean and standard deviation are roughly twice as large.

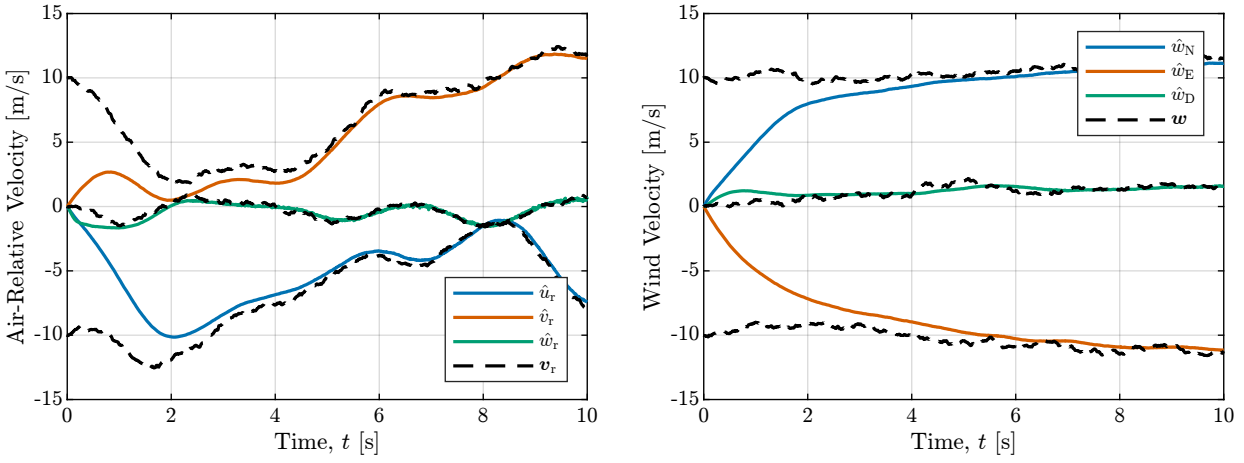

(a) Air-relative velocity **(b) Wind velocity**

Fig. 11 Sample time history of state estimates using the optimal bounds tuning approach.

VI. Conclusions

A stochastic symmetry-preserving, reduced-order observer has been developed to estimate wind from aircraft motion in turbulence. Leveraging the invariance of the stochastic aircraft dynamics under Lie group actions, the proposed observer achieves linear error dynamics, enabling the application of standard observer/estimator design techniques, such as Kalman-Bucy filtering. Noise-to-state stability guarantees provide probabilistic bounds on the convergence of the invariant error, although Monte-Carlo simulation revealed these bounds to be conservative. To address this, an

alternative tuning approach was explored, offering less conservative bounds at the cost of poorer transient performance. Future work will aim to obtain tighter bounds across various aircraft types (fixed-wing, multirotor, vertical takeoff and landing). More physically accurate turbulence models will be considered along with experimental validation using flight test data. By providing principled convergence guarantees, the proposed observer has the potential to support safety-critical systems by providing provably accurate extended state estimates that enable enhanced autonomy.

Appendix: A Note on State Observers versus State Estimators

Consider a dynamical system (possibly random) with state space $\mathcal{X}$ and observation space $\mathcal{Y}$. In short, we consider a *state estimate* to be the output of a mapping from $\mathcal{Y}$ to functions on $\mathcal{X}$. State estimates may be obtained from *state observers* or *state estimators*, for which we make a distinction. Consider a dynamical control system represented by differential equations of the form $\dot{\boldsymbol{x}} = \boldsymbol{f}(\boldsymbol{x}, \boldsymbol{u}) + \boldsymbol{g}(\boldsymbol{x}, \boldsymbol{u})\boldsymbol{w}$ where $\boldsymbol{x} \in \mathcal{X}$ is the state vector, $\boldsymbol{u} \in \mathcal{U}$ is the known control input, and $\boldsymbol{w} \in \mathcal{W}$ is an unknown disturbance (possibly random). Let $\boldsymbol{y} = \boldsymbol{h}(\boldsymbol{x}, \boldsymbol{u}) + \boldsymbol{d}(\boldsymbol{x}, \boldsymbol{u})\boldsymbol{v}$ be the measured outputs of the system, where $\boldsymbol{v} \in \mathcal{V}$ is an unknown measurement disturbance (possibly random).

The dynamical system $\dot{\boldsymbol{z}} = \boldsymbol{\alpha}(\boldsymbol{z}, \boldsymbol{y}, \boldsymbol{u})$ with the corresponding state estimate $\hat{\boldsymbol{x}} = \boldsymbol{\rho}(\boldsymbol{z}, \boldsymbol{y}, \boldsymbol{u})$ is considered a *state observer* if some stability claim can be made about the set $\mathcal{E} = \{(\boldsymbol{x}, \boldsymbol{z}) \mid \boldsymbol{x} = \hat{\boldsymbol{x}}\}$. The stability of $\mathcal{E}$ may be *asymptotic*, *input-to-state*, *stochastic*, *noise-to-state*, etc. Examples of state observers include linear Luenberger observers, H_∞ filters, passivity-based observers, high-gain observers, and the symmetry-preserving reduced-order observer considered in this paper.

A *state estimator* is not concerned with the stability of a state estimate, but rather with producing an informed mapping from measurements to *statistics* of points in the state space. Such statistics include the conditional mean $\hat{\boldsymbol{x}} = \mathbb{E}\{\boldsymbol{x}(t)|\{\boldsymbol{y}(\tau)\}_{\tau \leq t}\}$, the conditional covariance $\mathbb{E}\{[\boldsymbol{x}(t) - \hat{\boldsymbol{x}}(t)][\boldsymbol{x}(t) - \hat{\boldsymbol{x}}(t)]^\mathsf{T}|\{\boldsymbol{y}(\tau)\}_{\tau \leq t}\}$, or even the conditional probability density function $p(\boldsymbol{x}(t)|\{\boldsymbol{y}(\tau)\}_{\tau \leq t})$. Examples of state estimators include the Kalman filter, unscented Kalman filter, exact nonlinear filters (see [49] for examples), and particle filters. It is important to note that state estimators can also be state observers. For example, the Kalman filter can also be shown to be a noise-to-state stable observer.

Acknowledgments

The authors gratefully acknowledge NASA under Grant No. 80NSSC20M0162.

References

[1] Lie, F. A. P., and Gebre-Egziabher, D., "Synthetic Air Data System," *Journal of Aircraft*, Vol. 50, No. 4, 2013, pp. 1234–1249. https://doi.org/10.2514/1.C032177.

[2] Sun, K., Regan, C. D., and Gebre-Egziabher, D., "Observability and Performance Analysis of a Model-Free Synthetic Air Data Estimator," *Journal of Aircraft*, Vol. 56, No. 4, 2019, pp. 1471–1486. https://doi.org/10.2514/1.C035290.

[3] Lawrance, N. R., and Sukkarieh, S., "Path Planning for Autonomous Soaring Flight in Dynamic Wind Fields," *2011 IEEE International Conference on Robotics and Automation*, IEEE, Shanghai, China, 2011, pp. 2499–2505. https://doi.org/10.1109/ICRA.2011.5979966.

[4] Yang, S., and Jeon, S., "Recursive Path Planning and Wind Field Estimation for Precision Airdrop," *Journal of Guidance, Control, and Dynamics*, Vol. 42, No. 6, 2019, pp. 1429–1437. https://doi.org/10.2514/1.G003944.

[5] Gahan, K. C., Hopwood, J. W., and Woolsey, C. A., "Uncertainty in Wind Estimates, Part 1: Analysis Using Generalized Polynomial Chaos," *AIAA SCITECH 2024 Forum*, American Institute of Aeronautics and Astronautics, Orlando, FL, 2024. https://doi.org/10.2514/6.2024-2824.

[6] Hopwood, J. W., and Woolsey, C. A., "Passivity-Based Wind Estimation for Aircraft Maneuvering in Steady and Uniform Wind Fields," *AIAA SCITECH 2024 Forum*, American Institute of Aeronautics and Astronautics, Orlando, FL, 2024. https://doi.org/10.2514/6.2024-2654.

[7] Mahapatra, P., and Zrnic, D., "Sensors and Systems to Enhance Aviation Safety against Weather Hazards," *Proceedings of the IEEE*, Vol. 79, No. 9, 1991, pp. 1234–1267. https://doi.org/10.1109/5.97295.

[8] Stratton, D., and Stengel, R., "Real-Time Decision Aiding: Aircraft Guidance for Wind Shear Avoidance," *IEEE Transactions on Aerospace and Electronic Systems*, Vol. 31, No. 1, 1995, pp. 117–124. https://doi.org/10.1109/7.366298.

[9] Palomaki, R. T., Rose, N. T., van den Bossche, M., Sherman, T. J., and De Wekker, S. F. J., "Wind Estimation in the Lower Atmosphere Using Multirotor Aircraft," *Journal of Atmospheric and Oceanic Technology*, Vol. 34, No. 5, 2017, pp. 1183–1191. https://doi.org/10.1175/JTECH-D-16-0177.1.

[10] Trub, R., Moser, D., Schafer, M., Pinheiro, R., and Lenders, V., "Monitoring Meteorological Parameters with Crowdsourced Air Traffic Control Data," *2018 17th ACM/IEEE International Conference on Information Processing in Sensor Networks (IPSN)*, IEEE, Porto, 2018, pp. 25–36. https://doi.org/10.1109/IPSN.2018.00010.

[11] Jacob, J., Chilson, P., Houston, A., and Smith, S., "Considerations for Atmospheric Measurements with Small Unmanned Aircraft Systems," *Atmosphere*, Vol. 9, No. 7, 2018, p. 252. https://doi.org/10.3390/atmos9070252.

[12] Barbieri, L., Kral, S., Bailey, S., Frazier, A., Jacob, J., Reuder, J., Brus, D., Chilson, P., Crick, C., Detweiler, C., Doddi, A., Elston, J., Foroutan, H., González-Rocha, J., Greene, B., Guzman, M., Houston, A., Islam, A., Kemppinen, O., Lawrence, D., Pillar-Little, E., Ross, S., Sama, M., Schmale, D., Schuyler, T., Shankar, A., Smith, S., Waugh, S., Dixon, C., Borenstein, S., and de Boer, G., "Intercomparison of Small Unmanned Aircraft System (sUAS) Measurements for Atmospheric Science during the LAPSE-RATE Campaign," *Sensors*, Vol. 19, No. 9, 2019, p. 2179. https://doi.org/10.3390/s19092179.

[13] Adkins, K. A., Akbas, M., and Compere, M., "Real-Time Urban Weather Observations for Urban Air Mobility," *International Journal of Aviation, Aeronautics, and Aerospace*, Vol. 7, No. 4, 2020. https://doi.org/10.15394/ijaaa.2020.1540.

[14] Reiche, C., Cohen, A. P., and Fernando, C., "An Initial Assessment of the Potential Weather Barriers of Urban Air Mobility," *IEEE Transactions on Intelligent Transportation Systems*, Vol. 22, No. 9, 2021, pp. 6018–6027. https://doi.org/10.1109/TITS.2020.3048364.

[15] Thipphavong, D. P., Apaza, R., Barmore, B., Battiste, V., Burian, B., Dao, Q., Feary, M., Go, S., Goodrich, K. H., Homola, J., Idris, H. R., Kopardekar, P. H., Lachter, J. B., Neogi, N. A., Ng, H. K., Oseguera-Lohr, R. M., Patterson, M. D., and Verma, S. A., "Urban Air Mobility Airspace Integration Concepts and Considerations," *2018 Aviation Technology, Integration, and Operations Conference*, American Institute of Aeronautics and Astronautics, Atlanta, Georgia, 2018. https://doi.org/10.2514/6.2018-3676.

[16] Karr, D. A., Wing, D. J., Barney, T. L., Sharma, V., Etherington, T. J., and Sturdy, J. L., "Initial Design Guidelines for Onboard Automation of Flight Path Management," *AIAA AVIATION Forum*, VIRTUAL EVENT, 2021. https://doi.org/10.2514/6.2021-2326.

[17] González-Rocha, J., Woolsey, C. A., Sultan, C., and De Wekker, S. F. J., "Sensing Wind from Quadrotor Motion," *Journal of Guidance, Control, and Dynamics*, Vol. 42, No. 4, 2019, pp. 836–852. https://doi.org/10.2514/1.G003542.

[18] Gahan, K., Hopwood, J. W., and Woolsey, C. A., "Wind Estimation Using an H∞ Filter with Fixed-Wing Aircraft Flight Test Results," *AIAA SCITECH 2023 Forum*, American Institute of Aeronautics and Astronautics, National Harbor, MD & Online, 2023. https://doi.org/10.2514/6.2023-2252.

[19] Halefom, M. H., Hopwood, J. W., and Woolsey, C. A., "Unsteady Aerodynamics in Model-Based Wind Estimation from Fixed-Wing Aircraft Motion," *Journal of Guidance, Control, and Dynamics*, Vol. 47, No. 8, 2024, pp. 1556–1568. https://doi.org/10.2514/1.G007836.

[20] Reif, K., Gunther, S., Yaz, E., and Unbehauen, R., "Stochastic Stability of the Discrete-Time Extended Kalman Filter," *IEEE Transactions on Automatic Control*, Vol. 44, No. 4, 1999, pp. 714–728. https://doi.org/10.1109/9.754809.

[21] Krener, A. J., "The Convergence of the Extended Kalman Filter," *Directions in Mathematical Systems Theory and Optimization*, Vol. 286, edited by A. Rantzer and C. I. Byrnes, Springer Berlin Heidelberg, Berlin, Heidelberg, 2003, pp. 173–182.

[22] Chen, H., Bai, H., and Taylor, C. N., "Invariant-EKF Design for Quadcopter Wind Estimation," *2022 American Control Conference (ACC)*, IEEE, Atlanta, GA, USA, 2022, pp. 1236–1241. https://doi.org/10.23919/ACC53348.2022.9867417.

[23] Ahmed, Z., and Woolsey, C. A., "The Invariant Extended Kalman Filter for Wind Estimation Using a Small Fixed-Wing UAV in Horizontal-Plane Flight," *AIAA SCITECH 2024 Forum*, American Institute of Aeronautics and Astronautics, Orlando, FL, 2024. https://doi.org/10.2514/6.2024-2656.

[24] Etkin, B., *Dynamics of Atmospheric Flight*, Wiley, New York, 1972.

[25] Etkin, B., "Turbulent Wind and Its Effect on Flight," *Journal of Aircraft*, Vol. 18, No. 5, 1981, pp. 327–345. https://doi.org/10.2514/3.57498.

[26] Karagiannis, D., and Astolfi, A., "Nonlinear Observer Design Using Invariant Manifolds and Applications," *Proceedings of the 44th IEEE Conference on Decision and Control*, IEEE, Seville, Spain, 2005, pp. 7775–7780. https://doi.org/10.1109/CDC.2005.1583418.

[27] Astolfi, A., Karagiannis, D., and Ortega, R., "Chapter 5: Reduced-order Observers," *Nonlinear and Adaptive Control with Applications*, Communications and Control Engineering, Springer-Verlag, London, 2008, pp. 91–114.

[28] Hopwood, J., and Woolsey, C., "A Symmetry-Preserving Reduced-Order Observer," *2025 American Control Conference*, Denver, Colorado, 2025. https://doi.org/10.48550/arXiv.2411.07998.

[29] Bonnabel, S., Martin, P., and Rouchon, P., "Symmetry-Preserving Observers," *IEEE Transactions on Automatic Control*, Vol. 53, No. 11, 2008, pp. 2514–2526. https://doi.org/10.1109/TAC.2008.2006929.

[30] Mateos-Núñez, D., and Cortés, J., "Pth Moment Noise-to-State Stability of Stochastic Differential Equations with Persistent Noise," *SIAM Journal on Control and Optimization*, Vol. 52, No. 4, 2014, pp. 2399–2421. https://doi.org/10.1137/130924652.

[31] Holm, D. D., Schmah, T., and Stoica, C., *Geometric Mechanics and Symmetry: From Finite to Infinite Dimensions*, Oxford Texts in Applied and Engineering Mathematics, Oxford University Press, New York, 2009.

[32] Morelli, E. A., and Klein, V., *Aircraft System Identification: Theory and Practice*, 2nd ed., Sunflyte Enterprises, Williamsburg, Virginia, 2016.

[33] Arnold, L., *Stochastic Differential Equations: Theory and Applications*, Wiley, New York, 1974.

[34] Evans, L. C., *An Introduction to Stochastic Differential Equations*, 1st ed., American Mathematical Society, Providence, RI, 2013.

[35] Gliklikh, Y. E., *Ordinary and Stochastic Differential Geometry as a Tool for Mathematical Physics*, Springer Netherlands, Dordrecht, 1996. https://doi.org/10.1007/978-94-015-8634-4.

[36] Olver, P. J., *Classical Invariant Theory*, 1st ed., Cambridge University Press, 1999. https://doi.org/10.1017/CBO9780511623660.

[37] Boothby, W. M., *An Introduction to Differentiable Manifolds and Riemannian Geometry*, revised second edition ed., Academic Press, San Diego, 2003.

[38] Pavliotis, G. A., *Stochastic Processes and Applications: Diffusion Processes, the Fokker-Planck and Langevin Equations*, Texts in Applied Mathematics, Vol. 60, Springer New York, New York, NY, 2014. https://doi.org/10.1007/978-1-4939-1323-7.

[39] Gaeta, G., and Lunini, C., "On Lie-point Symmetries for Ito Stochastic Differential Equations," *Journal of Nonlinear Mathematical Physics*, Vol. 24, No. Supplement 1, 2017, pp. 90–102. https://doi.org/10.1080/14029251.2017.1418056.

[40] Hopwood, J. W., and Woolsey, C. A., "Nonlinear Wind Estimation Using a Symmetry-Preserving Reduced-Order Observer," *AIAA SCITECH 2025 Forum*, American Institute of Aeronautics and Astronautics, Orlando, FL, 2025.

[41] Khalil, H. K., *Nonlinear Systems*, 2nd ed., Prentice Hall, Upper Saddle Ridge, New Jersey, 1996.

[42] Borkar, V. S., *Probability Theory: An Advanced Course*, Springer, New York, 1995. https://doi.org/10.1007/978-1-4612-0791-7.

[43] Moylan, P., "A Note on Kalman-Bucy Filters with Zero Measurement Noise," *IEEE Transactions on Automatic Control*, Vol. 19, No. 3, 1974, pp. 263–264. https://doi.org/10.1109/TAC.1974.1100570.

[44] Anderson, B., "Stability Properties of Kalman-Bucy Filters," *Journal of the Franklin Institute*, Vol. 291, No. 2, 1971, pp. 137–144. https://doi.org/10.1016/0016-0032(71)90016-0.

[45] Grauer, J. A., and Morelli, E. A., "Generic Global Aerodynamic Model for Aircraft," *Journal of Aircraft*, Vol. 52, No. 1, 2015, pp. 13–20. https://doi.org/10.2514/1.C032888.

[46] Hopwood, J. W., Simmons, B. M., Woolsey, C. A., and Cooper, J. K., "Development and Evaluation of Multirotor Flight Dynamic Models for Estimation and Control," *AIAA SCITECH 2024 Forum*, American Institute of Aeronautics and Astronautics, Orlando, FL, 2024. https://doi.org/10.2514/6.2024-1307.

[47] Kloeden, P. E., and Platen, E., *Numerical Solution of Stochastic Differential Equations*, Springer Berlin Heidelberg, Berlin, Heidelberg, 1992. https://doi.org/10.1007/978-3-662-12616-5.

[48] Rugh, W. J., *Linear System Theory*, 2nd ed., Prentice Hall Information and System Sciences Series, Prentice Hall, Upper Saddle River, N.J, 1996.

[49] Daum, F., "Nonlinear Filters: Beyond the Kalman Filter," *IEEE Aerospace and Electronic Systems Magazine*, Vol. 20, No. 8, 2005, pp. 57–69. https://doi.org/10.1109/MAES.2005.1499276.